

MIT Open Access Articles

Unifying Exchange Sensitivity in Transition-Metal Spin-State Ordering and Catalysis through Bond Valence Metrics

The MIT Faculty has made this article openly available. **Please share** how this access benefits you. Your story matters.

Citation: Gani, Terry Z. H. and Heather J. Kulik. "Unifying Exchange Sensitivity in Transition-Metal Spin-State Ordering and Catalysis through Bond Valence Metrics." *Journal of Chemical Theory and Computation* 13, 11 (October 2017): 5443-5457 © 2017 American Chemical Society

As Published: <http://dx.doi.org/10.1021/acs.jctc.7b00848>

Publisher: American Chemical Society (ACS)

Persistent URL: <https://hdl.handle.net/1721.1/123834>

Version: Author's final manuscript: final author's manuscript post peer review, without publisher's formatting or copy editing

Terms of Use: Article is made available in accordance with the publisher's policy and may be subject to US copyright law. Please refer to the publisher's site for terms of use.



Unifying Exchange Sensitivity in Transition Metal Spin-State Ordering and Catalysis Through Bond Valence Metrics

Terry Z. H. Gani¹ and Heather J. Kulik^{1,*}

¹*Department of Chemical Engineering, Massachusetts Institute of Technology, Cambridge, MA*

02139

ABSTRACT: Accurate predictions of spin-state ordering, reaction energetics, and barrier heights are critical for the computational discovery of open-shell transition metal (TM) catalysts. Semilocal approximations in density functional theory, such as the generalized gradient approximation (GGA), suffer from delocalization error that causes them to overstabilize strongly bonded states. Descriptions of energetics and bonding are often improved by introducing a fraction of exact exchange (e.g., erroneous low-spin GGA ground states instead correctly predicted as high-spin with a hybrid functional). The degree of spin-splitting sensitivity to exchange can be understood based on the chemical composition of the complex, but the effect of exchange on reaction energetics in a single spin state is less well-established. Across a number of model iron complexes, we observe strong exchange sensitivities of reaction barriers and energies that are of the same magnitude as those for spin splitting energies. We rationalize trends in both reaction and spin energetics by introducing a measure of delocalization, the bond valence of the metal-ligand bonds in each complex. The bond valence represents a simple-to-compute property that unifies understanding of exchange sensitivity for catalytic properties and spin-state ordering in TM complexes. Close agreement of the resulting per-metal-organic-bond sensitivity estimates, together with failure of alternative descriptors demonstrates the utility of the bond valence as a robust descriptor of how differences in metal-ligand delocalization produce differing relative energetics with exchange tuning. Our unified description explains the overall effect of exact exchange tuning on the paradigmatic two-state FeO/CH₄ reaction that combines challenges of spin-state and reactivity predictions. This new descriptor-sensitivity relationship provides a path to quantifying how predictions in transition metal complex screening are sensitive to the method used.

1. Introduction

The promise of open shell transition metal (TM) complexes, e.g., for the selective activation of hydrocarbons, has motivated first-principles screening for understanding catalytic action and designing improved catalysts^{1,4}. Approximate density functional theory (DFT) is widely used for the mechanistic study of TM complexes, but presently available exchange-correlation approximations in DFT are plagued by both one- and many-electron self-interaction errors^{5,9}, also referred to as delocalization error¹⁰⁻¹². Mechanistic predictions in open-shell TM catalysis¹³ are particularly sensitive to these delocalization errors, which reduce accuracy in both calculated bond dissociation energies (BDEs)^{6,14-17} and barrier heights¹⁸ within a given spin state as well as the relative energetic ordering of spin states^{19,24}.

The delocalization error in a semi-local (e.g., generalized gradient approximation, GGA) functional stabilizes overly-delocalized, covalent states²⁵ and generally gives rise to poor energetics¹³, such as favoring more bonded interactions in low-spin (LS) than in high-spin (HS) states^{24, 26-28}. Strategies that aim to recover the derivative discontinuity²⁹ lacking from GGA functionals^{5, 30-35} include tuned hybrids^{25, 36-45}, DFT+U^{26, 46-48}, and self-interaction corrections⁴⁹⁻⁵¹. These approaches generally behave similarly in TM catalysts by decreasing covalency²⁵ with respect to GGAs. This consistent effect is observed through electron density localization away from the metal and onto ligand states⁵² and decreased dative bonding in inorganic complexes^{45, 53-55}.

By construction, DFT+U^{26, 46-48} directly penalizes hybridization in metal-ligand bonding orbitals²⁶, improving transition metal catalysis predictions^{19, 56}. However, this approach necessitates self-consistent⁹ or HF-based⁵⁷ calculation of a Hubbard U parameter that should be allowed to vary⁵⁸ across the reaction coordinate. Like other approximations, DFT+U can be shown⁵⁹ to recover the derivative discontinuity²⁹ in approximate DFT but not at a U value that corresponds to the self-consistently calculated one⁵⁹.

Hybrid functionals, which incorporate an admixture of Hartree-Fock (HF) exchange, provide a straightforward approach in practical DFT to correct delocalization errors⁶⁰, and HF exchange is one of the most frequently tuned parameters when a functional is selected for DFT study.

However, the fraction of HF exchange required, as judged by comparison to experiment or accurate-but-computationally-expensive correlated wavefunction theory (WFT) reference, is strongly dependent on the system^{20-22, 61-63} and, to a lesser extent, on the parameterization of the GGA exchange-correlation functional⁶⁴. Incorporation of HF exchange reduces dissociation energies in TM compounds⁶⁵ and can influence energies of isomers⁶⁶. For equilibrium energetics and BDEs, low fractions of HF exchange have been motivated by benchmark studies of TM dimers and diatomics^{65, 67-71}, possibly owing to the larger relevance⁷¹⁻⁷² of static correlation error^s in these systems. Conversely, higher HF exchange fractions have been motivated by studies of larger TM complexes⁷³.

The effect of HF exchange on spin-state ordering is very well-studied, although leading to conflicting proposals of low^{70, 74-75} and high^{71, 76-77} percentages for the accurate description of spin-state ordering. Increasing HF exchange on octahedral complexes reverses the GGA preference for LS states to instead favor HS states in a roughly linear fashion^{20-22, 61, 74-75, 78}. The spin-state ordering sensitivity to HF exchange is correlated to the ligand field strength of coordinating ligands^{22, 61}, with bare ions exhibiting dramatically reduced sensitivities²⁴. Between LS and HS equilibrium geometries, vertical spin splitting sensitivities increase with the metal-ligand bond length⁷⁹, approaching the adiabatic spin splitting sensitivity when evaluated at the HS geometry⁸⁰. If GGA errors are comparable across complexes, higher sensitivities to HF exchange in some cases likely explain why differing prescriptions of HF exchange are recommended in the literature. Building upon these initial observations of structure-sensitivity relationships, our group recently developed a neural network that predicts the exchange sensitivity of spin-state splitting based only on the catalyst's composition, enabling no-cost extrapolation to results for B3LYP and higher exchange fractions from a semi-local GGA calculation.⁸⁰

The correct functional choice and amount of HF exchange that should be used in modeling catalytic cycles^{69, 74, 78} remains even less clear than for the case of spin-state ordering. Poor functional choice for a given reaction has yielded unphysical mechanistic predictions, such as barrierless hydrogen abstraction⁸¹, spurious complex-substrate charge transfer⁸¹⁻⁸² or identification

of the wrong reactive spin surface⁸³. Uncertainty quantification⁸⁴⁻⁸⁶ from statistical analysis of an ensemble of functionals can be used as a tool to introduce confidence intervals to catalytic predictions for a single catalyst or cycle if a suitable ensemble of functionals is chosen. Complementary to this approach, a broader understanding of prediction sensitivity to the most commonly varied functional parameters is needed in computational catalysis. Unlike spin-state splitting, relationships between catalytic intermediate structure and either exchange sensitivity or semi-local DFT errors are not yet well known.

In this work, we determine the relative HF exchange sensitivities of spin-state splitting and catalytic steps in representative alkane hydroxylation catalytic cycles involving open-shell TM complexes. We introduce a new metric based on the relative degree of metal-ligand bonding between spin-states or catalytic intermediates being compared (i.e., the change in bond valence or BV). We employ this new quantity to provide a unified rationalization of exchange sensitivity in reaction free energies, barrier heights, and spin-state ordering of TM complexes. We show this metric is applicable to catalytic cycles with and without changes in oxidation state and spin state. Combined with accurate WFT references, we are able to provide a clearer view of why no presently available functional is likely to accurately describe an entire catalytic cycle. The rest of this manuscript is as follows. In section 2, we provide the Computational Details of the calculations employed in this work including the definition of the BV metric. In section 3, we present Results and Discussion on exchange sensitivities in catalysis and spin-state splitting as well as their relationship to BV changes. Finally, in section 4, we provide our Conclusions.

2. Computational Details

Density functional theory (DFT). All DFT single-point energy calculations, frequency calculations, and geometry optimizations were performed with a development version of the TeraChem⁸⁷⁻⁸⁸ graphical processing unit (GPU)-accelerated quantum chemistry package. All calculations were spin-unrestricted and use the composite LACVP* basis set, which consists of the LANL2DZ effective core potential⁸⁹⁻⁹⁰ for Fe and Zn and the 6-31G* basis set for all other atoms. This modest basis set was found to be accurate in our previous work⁹¹ on TM complex

redox and spin-state energetics due to cancellation of error, but larger basis sets nevertheless yield comparable sensitivities on representative cases (see Supporting Information Table S1 and Figure S1).

The effect of exact exchange was investigated by altering²² the percentage of HF exchange in a modified form of the B3LYP^{92,94} global hybrid functional that was augmented with the empirical DFT-D3 correction⁹⁵ from as low as 10% to as high as 30% HF exchange in increments of 10%, unless otherwise noted. The D3 correction has no effect on computed sensitivities or BVs (Supporting Information Table S2). We employ the following modified²² B3LYP exchange expression:

$$E_x^{\text{modB3LYP}} = E_x^{\text{LDA}} + a_0(E_x^{\text{HF}} - E_x^{\text{LDA}}) + 0.9(1 - a_0)(E_x^{\text{GGA}} - E_x^{\text{LDA}}) \quad (1)$$

while holding the GGA/LDA ratio fixed to the 9:1 value in standard B3LYP^{92,94}. This choice is motivated by the widespread use of B3LYP in the community along with our earlier observations of universal effects of HF exchange tuning in other GGAs.²²

The default definition of B3LYP in TeraChem employs the VWN1-RPA form for the LDA VWN⁹⁶ component of LYP⁹³ correlation, and the default D3 correction used includes Becke-Johnson damping⁹⁷. To facilitate quantitative comparison of the effect of varying HF exchange fraction across reactions, we introduce linear fits as approximations to the reaction energy sensitivities (S), i.e., the partial derivatives of the reaction energies with respect to HF exchange fraction (a_{HF}), extending a concept that we have previously applied to spin-splitting energies²² and partial charges²²:

$$\text{slope} = S_r = \frac{\Delta\Delta E_r}{\Delta a_{\text{HF}}} \approx \frac{\partial\Delta E_r}{\partial a_{\text{HF}}} \quad (2)$$

where the unit notation “HFx”²² is used to represent the range from 0 to 100% HF exchange. Unless otherwise noted, all S values are evaluated using a central difference approximation centered at 20% HF exchange (i.e., B3LYP) and ranging from 10 to 30% HF exchange, and

correlated against properties evaluated at 20% HF exchange. This procedure is only meaningful if the dependence of ΔE_i on HFX is approximately linear, which is the case in the majority of reactions studied in this work. We discuss sources and degrees of nonlinearity in Sec. 3d.

Although commonly proposed values of HF exchange for TM complexes in the literature range from around 0%^{20, 74-75} to 40-50%^{21, 76-77}, we consider a sensitivity to be chemically meaningful only if $\Delta\Delta E_i$ changes by more than 3 kcal/mol (i.e., outside of chemical accuracy for TM complexes⁹⁸) over a range of 0.156 HFX (corresponding to a 3σ confidence interval²² on the normal distribution fit to the votes for standard hybrid functionals in a popular DFT poll⁹⁹), i.e.,

$$S > 19 \frac{\text{kcal}}{\text{mol} \cdot \text{HFX}} .$$

Geometry optimizations used the L-BFGS algorithm in translation rotation internal coordinates (TRIC)¹⁰⁰ as implemented in a development version of TeraChem⁸⁷⁻⁸⁸ to the default tolerances of 4.5×10^{-4} hartree/bohr for the maximum gradient and 1×10^{-6} hartree for the change in self consistent field (SCF) energy between steps. All structures were separately optimized at each HF exchange value studied unless otherwise stated. Initial guess geometries were generated with the molSimplify¹⁰¹ toolkit using trained⁸⁰ metal-ligand bond distances. A list of all TM complexes studied in this work are provided in Supporting Information Table S3 and their optimized geometries are provided in the Supporting Information attached xyz files.

Transition states (TSs) were obtained with partitioned rational function optimization (P-RFO)¹⁰² at the B3LYP/DFT-D3/LACVP* level of theory using QChem 4.4¹⁰³, as an analytic Hessian for TS optimization is not implemented in TeraChem. All TSs were characterized with vibrational frequency analysis to confirm a single imaginary frequency, followed by reaction path analysis¹⁰⁴⁻¹⁰⁵ using the intrinsic reaction coordinate (IRC)¹⁰⁶⁻¹⁰⁷. TeraChem⁸⁷⁻⁸⁸ single-point energy calculations on the resulting structures obtained from QChem were obtained to enable direct energy comparisons between intermediates and TSs.

Vertical ionization potentials (IPs) were calculated by taking the difference in electronic

energies of the oxidized and ground-state species, both evaluated at the ground-state optimized geometry unless otherwise noted:

$$\text{IP}(X^{n+}) = E(X^{(n+1)+}) - E(X^{n+}) \quad (3)$$

Correlated wavefunction theory (WFT). WFT reference energetics for the oxo formation reaction step were computed with domain based local pair-natural orbital coupled-cluster theory (DLPNO-CCSD(T))¹⁰⁸. These calculations were performed with ORCA 4.0¹⁰⁹ on DFT-optimized structures using the aug-cc-pVDZ and aug-cc-pVTZ basis sets, automatically generated¹¹⁰ auxiliary basis sets, and default values were used for pair cutoffs. Extrapolation to the complete basis set (CBS) limit^{111,112} was performed using the formulas in ref. 113. The degree of multireference (MR) character, as measured by the largest pair natural orbital (PNO) amplitude¹¹⁴, remains low over the oxo formation reaction coordinate, increasing from 0.07 in the reacting complex (RC) to 0.10 in the TS and 0.25 in the product complex (PC) (Supporting Information Table S4). To justify our use of a single-reference method for this reaction step, we also computed NEVPT2¹¹⁵ energies for the RC and PC. NEVPT2 calculations were performed with ORCA 4.0¹⁰⁹ using the def2-TZVPP¹¹⁶ basis set and following details in ref. 117. We used an active space of 10 electrons in 12 orbitals for the RC, which is an octahedral Fe(II) complex with weakly bound ligands. This active space consists of five Fe 3*d* orbitals, the bonding counterparts to the 3*d*_{x²-y² and 3*d*_{z²} orbitals, and the 4*d*_{xy}, 4*d*_{xz} and 4*d*_{yz} orbitals to account for the double-shell effect.¹¹⁸ We omitted the 4*d*_{x²-y²} and 4*d*_{z²} orbitals¹¹⁷ to maintain consistency with the other active spaces. For the PC, which is an Fe(IV)-oxo complex, we used an active space of 12 electrons in 12 orbitals consisting of the orbitals in the RC active space and the O 2*p*_x and 2*p*_y orbitals¹¹⁷.}

For hydrogen atom transfer (HAT), strong MR character caused by spin coupling of the methyl radical and the iron-oxo species necessitates MR approaches such as NEVPT2¹¹⁵, which we have performed for the RC and the TS using active spaces of 12 electrons in 12 orbitals and 14 electrons in 14 orbitals, respectively¹¹⁷. The TS active space consists of the orbitals in the RC active space plus the $\sigma_{\text{CHO}}/\sigma_{\text{CHO}}^*$ bonding-antibonding pair, and the omission of the 4*d*_{x²-y²} and 4*d*_{z²}

orbitals is motivated by memory constraints¹¹⁷. The HAT PC, i.e., Fe(III)-OH-CH₃, was not considered due to the lack of a suitable literature active space.

Bond valences (BVs) and post-processing. For quantification of electron delocalization in metal-ligand bonds, we employ the Mayer bond order (I)¹¹⁹⁻¹²⁰, as calculated by Multiwfn¹²¹. This quantity is cheap to calculate and has been found useful for comparing bonding among 3d TM complexes¹²² as well as heavier complexes¹²³. The BV of an atom, here the TM center of a TM complex, is then defined as the sum of Mayer bond orders with all other atoms¹¹⁹:

$$BV_A = \sum_{B \neq A} I_{AB} \quad (4)$$

Comparisons with other measures of electron delocalization, including natural bond orbital (NBO)¹²⁴-derived bond orders and atoms-in-molecules (AIM)¹²⁵-derived quantities, are provided in Supporting Information Figure S2. Natural population analysis (NPA)¹²⁴-derived partial charges were obtained from the TeraChem interface with the NBO 6.0 package²⁶. Cube files and deformation density distributions were obtained with the Multiwfn post-processing package²¹ and projected onto the xy-plane for visualization.

3. Results and Discussion

3a. Model Catalytic Cycles.

To begin to understand the effect of HF exchange on catalytic cycles, we first consider CH₄ hydroxylation by a model Fe(II) complex. We use N₂O as the terminal oxidant¹²⁷, instead of O₂ as the paths to O₂ activation in synthetic complexes are less well-established¹²⁸⁻¹²⁹ (Figure 1). This process has attracted significant attention due to the importance of partial oxidations of abundant feedstocks¹³⁰ that are performed under mild conditions by highly-efficient and selective enzymes¹³¹⁻¹³². Unique aspects of open-shell TM complex electronic structure^{117, 133-134} require an understanding of how spin-state influences reactivity, leading to two-state reactivity (TSR)¹³⁵⁻¹³⁶ and exchange-enhanced reactivity (EER)¹³⁷⁻¹³⁸ models. For this first catalytic cycle, all calculations were performed on the ground state, HS quintet surface (TSR is discussed in Sec. 3d), and

inclusion of counter-ions to address unphysical charge delocalization^{81, 139} was found to be unnecessary here due to the higher IP of CH₄ vs. larger substrates such as cyclohexane^{82, 140}.

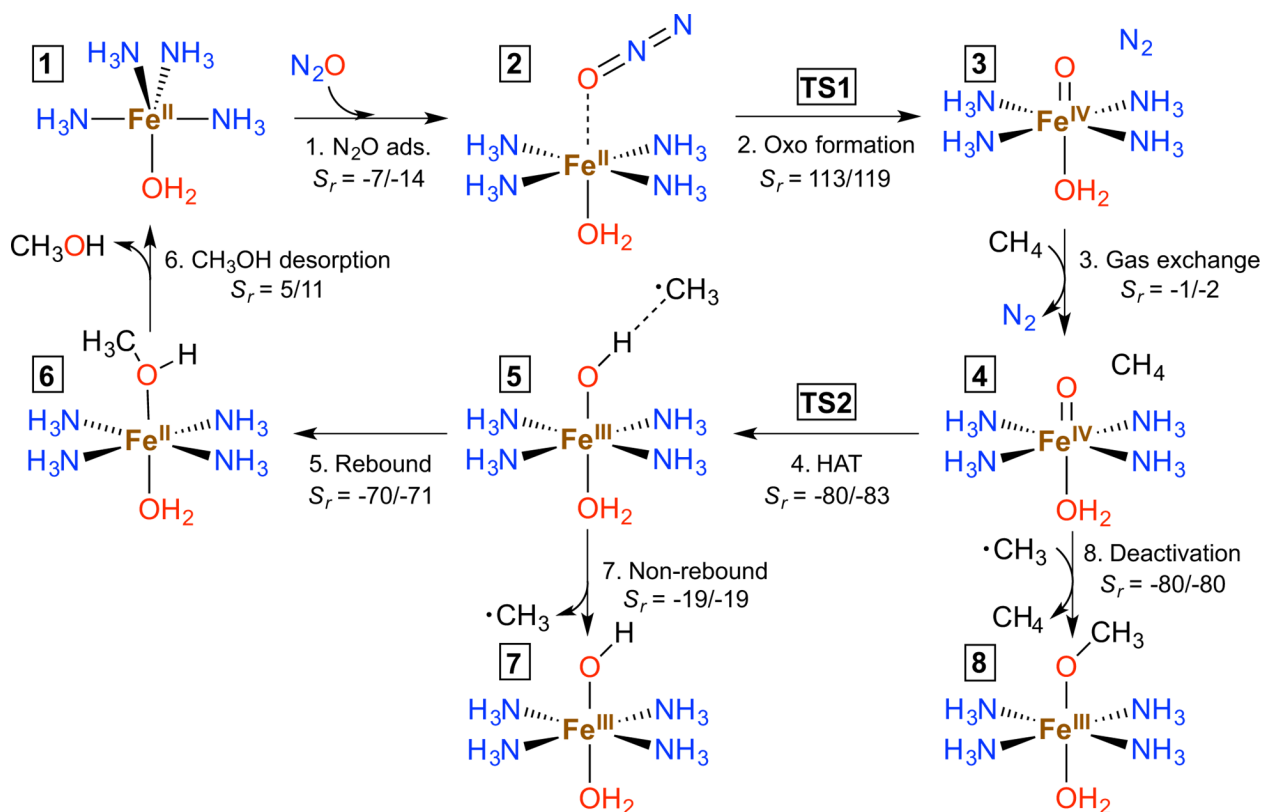


Figure 1. CH₄ hydroxylation by N₂O catalyzed by the model tetraammineiron(II) complex. All complexes have a charge of +2. The labels below each reaction step indicate the HF exchange sensitivities (S_r , units of kcal/molHFX) of electronic energy (left) and Gibbs free energy (right) changes. No TS could be found for step 5 (rebound) due to the large, negative reaction energy.

Within the framework of the energetic span model¹⁴¹, the turnover-determining TS (TDTS) and turnover-determining intermediate (TDI) in this catalytic cycle are the oxo-formation TS (**TS1**) and the Fe(II)-CH₃OH rebound intermediate (**6**) respectively, in agreement with previous mechanistic studies^{114, 142} (Figure 2). The magnitudes of S_r for individual steps vary widely, ranging from near zero in steps 1 and 6 to 113 kcal/molHFX in step 2 (Figure 1). All steps except steps 1, 3 and 6 have chemically meaningful S_r according to our criterion developed in Sec. 2. Both positive and negative S_r values are observed, and this results in divergent effects on the TDTS and TDI: increasing the amount of HF exchange in the functional destabilizes the

TDTS while stabilizing the TDI, increasing the energetic span and hence decreasing the computed turnover frequency (TOF) (Figure 2). Over the modest variation from 15 (e.g., in the reparametrized B3LYP* functional⁴⁴) to 25% HF exchange (e.g., in the PBE0 functional⁴³), the energetic span widens from 50 kcal/mol to 56 kcal/mol, which corresponds to a 5 order of magnitude decrease in the computed TOF at 298 K.

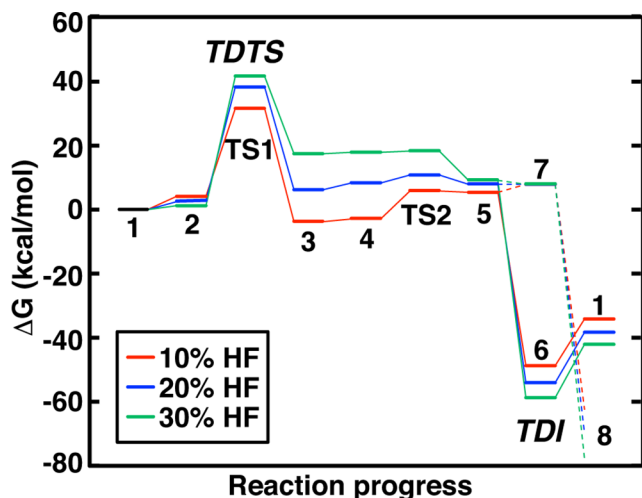


Figure 2. Energy level diagram for the Fe(II) model catalyst methane to methanol catalytic cycle intermediates shown schematically in Figure 1 computed at 10%, 20% and 30% HF exchange with the B3LYP functional. All curves have been aligned at intermediate 1, and the TDTS and TDI are labeled accordingly.

Considering the strong, yet systematic, dependence of computed observables such as the TOF with HF exchange fraction, a scheme for rationalizing and predicting these sensitivity differences is desirable for high-throughput catalyst screening workflows that rely on a single hybrid (or GGA) functional. To this end, similar sensitivity trends have been observed in other model alkane hydroxylation reactions^{81, 144} and attributed to changes in the oxidation number of Fe⁸¹, with an increase in oxidation number (e.g., Fe(III) to Fe(IV)) corresponding to increased sensitivity and vice versa. Although this simple model at first appears adequate for this system, it suffers from several shortcomings: (1) the oxidation number is formally only defined over integer values¹⁴⁵ and hence unable to take into account fractional bond orders, e.g., in TSs or weakly-bound ligands, (2) it does not distinguish between an increase in formal charge (e.g.,

through electron transfer) and electron delocalization (e.g., through additional metal-ligand bonds), and (3) assignment of oxidation numbers is ambiguous in all theoretical calculations but especially TM complexes with non-innocent ligands. Instead, we will show that the BV change we introduce in this work is a quantitative metric for HF sensitivity and addresses the shortcomings above: fractional bond orders are well-defined and physically meaningful, BV increases correlate to increased electron delocalization as bonding orbitals are more delocalized than nonbonding orbitals, and explicit assignment of electrons to metal or ligand is not required. At the same time, the change in BV reduces to the change in oxidation number if all bond orders are assumed to be integers.

As each step in this model catalytic cycle is fortuitously well-described by near-integer BV changes, the BV change and oxidation number are both suitable metrics for rationalizing relative HF exchange sensitivity of reaction steps. Plotting S_i of each reaction step against the change in total Fe BV yields a strong correlation ($R^2=0.94$) despite the fact that we have treated different bond types equivalently and ignored BV changes of the organic molecules themselves (Figure 3). We further discuss these effects in Sec. 3b. The value of the slope indicates that the formation of an Fe-X bond is disfavored by about 68 kcal/mol from 0% to full (i.e., 100% HF) exact exchange. Both the numerical value and quality of this fit are insensitive to basis set choice (see Supporting Information Table S1 and Figure S1). HF exchange in hybrid functionals has been observed to lower BDEs in TM compounds by 7-8 kcal/mol per 10% of HF exchange on average⁶⁵, which is in reasonable agreement with the computed slope. The largest deviations from this trend occur in the weakly-bound N₂O adsorption and CH₃OH dissociation steps, which are also sensitive to basis set size but have small S_i values (see Supporting Information Table S1 and Figure S1).

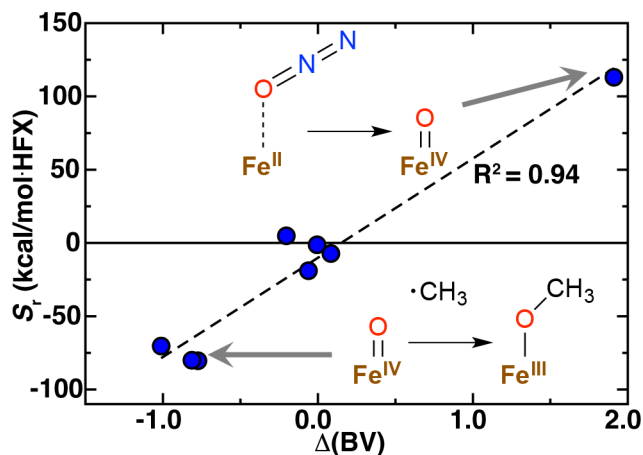


Figure 3. Dependence of reaction energy sensitivity to HF exchange (S_i) on the change in Fe bond valence (ΔBV) for each reaction step in Figure 1. Representative reaction steps with large positive and negative sensitivities are indicated with arrows.

It is useful to compare the HF exchange sensitivities of electronic energy changes (S_i) and Gibbs free energy changes ($S_{i,g}$), as ΔG_i rather than ΔE_i determines catalytic activity. Although vibrational frequencies increase with HF exchange and are systematically overestimated by pure HF and some hybrid functionals¹⁴⁶, this effect may be expected to largely cancel out in a chemical reaction, as most spectator vibrational modes in the reacting complex remain unchanged from reactants to products. Despite metal-ligand bond orders decreasing with increasing HF exchange, vibrational frequencies of the metal-ligand and other bonds in the complex generally increase (Supporting Information Figure S3). As a result, we observe a consistent, though slight, increase in magnitude of $S_{i,g}$ relative to S_i for all reaction steps in this catalytic cycle, and correlations of $S_{i,g}$ with change in total Fe BV are comparable ($R^2=0.93$, Supporting Information Figure S4). Hence, conclusions regarding HF exchange sensitivities of electronic energy changes are also applicable to Gibbs free energy changes, although it should be noted that the deviation from linearity for the computed sensitivities is increased due to changes in vibrational frequencies.

To investigate if our observations on the BV metric can be generalized to other catalytic cycles, we repeat this analysis on CO_2 hydration catalyzed by a Zn(II) biomimetic complex of carbonic anhydrase¹⁴⁷⁻¹⁴⁹ (Figure 4). To facilitate comparison to the previous example, we also consider the direct Fe(II) analogue. The Zn(II) complex is a closed-shell singlet whereas the

B3LYP ground state of the Fe(II) complex is an open-shell quintet (Supporting Information Table S5). The metal oxidation state remains constant as Zn(II) and Fe(II) in this catalytic cycle, and thus oxidation number cannot be used to predict exchange sensitivity. Sensitivities are much lower overall in both cases, with the most sensitive step having an S_r of 21 kcal/molHFX compared to 113 kcal/molHFX in the previous example. The deprotonation step (1 \rightarrow 2) is barrierless, and owing to low sensitivities, we did not carry out further analysis of the TS for the CO₂ insertion step (2 \rightarrow 3). Trends in these small but nonzero sensitivities can, however, still be rationalized by considering differences in BVs. Considering the most sensitive steps of the cycle, namely H₂O deprotonation and CO₂ insertion, we observe that the oxygen-containing ligand changes from neutral (H₂O) to anionic with high charge density (OH⁻) to anionic with delocalized charge (O⁻COOH). The corresponding changes in M-O bond strength are quantified by our BV measure and corroborated by bond length changes (Figure 4). The signs and relative magnitudes of S_r correspond well with the relative changes in BVs. The Fe(II) reaction steps are more sensitive than the corresponding Zn(II) reaction steps, which may be due to the reduced 3*d* character of bonding orbitals in Zn(II) owing to its closed shell *d*¹⁰ nature³⁹ (Supporting Information Figure S5).

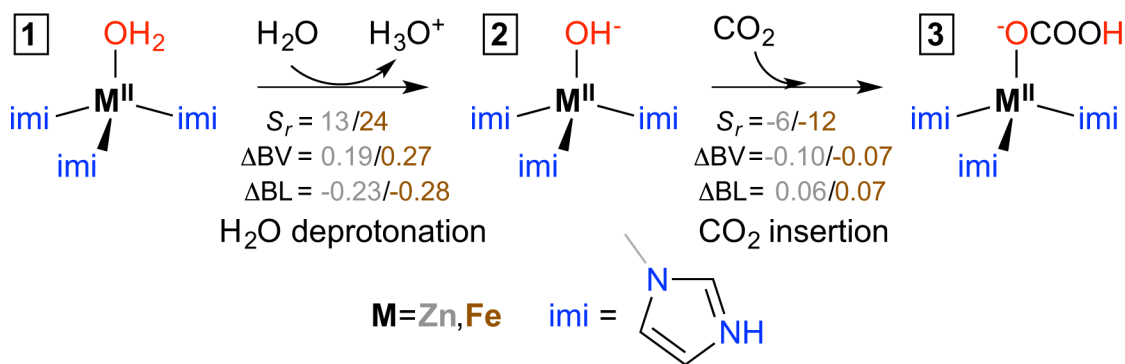


Figure 4. Key steps of CO₂ hydration catalyzed by a model Zn(II) complex and its Fe(II) analogue. The sensitivities of reaction energies with respect to HF exchange fraction (S_r , units of kcal/molHFX), M-O bond length changes (ΔBL , units of Å) and bond valence changes (ΔBV) for the two reaction steps (H₂O deprotonation and CO₂ insertion) are labeled accordingly, with the left and right values corresponding to Zn(II) and Fe(II) respectively. Due to their small absolute values, the reported S_r values have been corrected for the sensitivities of the uncatalyzed reaction steps (-2.5 kcal/molHFX and -7.5 kcal/molHFX respectively).

3b. Reaction Coordinates in a Model Catalyst.

We now consider the continuous variation of HF exchange sensitivity along reaction coordinates to determine if BV changes also explain sensitivity along chemical steps. We computed the B3LYP (20% exchange) IRC reaction paths for oxo formation and HAT reaction steps by proceeding down from the **TS** back to the respective reactant complex, **RC**, and forward to the product complex, **PC**, and also recomputed single point energies of these structures at 10% and 30% HF exchange (see structures in Figure 1). The energy profiles shift uniformly in a direction consistent with the sign of the overall S for the step, i.e., positive for oxo formation ($S = 113$ kcal/molHFX) and negative for HAT ($S = -80$ kcal/molHFX). This observation can be interpreted as a gradual increase in magnitude of the exchange sensitivity of total energies along the reaction coordinate (Figure 5). The net change in BV increases with reaction progress, providing a satisfactory, albeit qualitative, single descriptor that explains the observed energetic behavior (Supporting Information Figure S6). We note that for other catalytic cycles beyond the scope of this work, the BV change between the **RC** and **PC** could instead be small and reach a maximum in the **TS**, which would instead lead to a different sensitivity profile on the IRC.

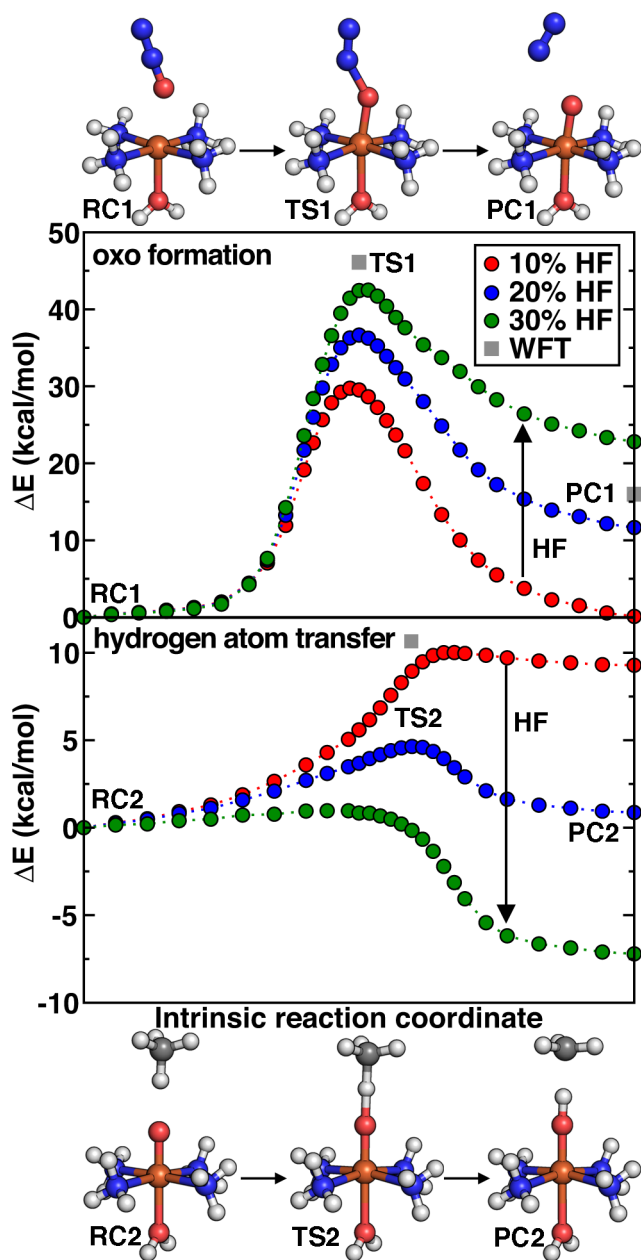


Figure 5. Energy profiles of the oxo formation (top) and hydrogen atom transfer (bottom) reaction steps computed at 10 (red circles), 20 (blue circles), and 30% (green circles) HF exchange. Structures were obtained along the B3LYP (20% HF exchange) IRC and single-point energies were recomputed at 10 and 30% HF exchange. Structures of the reacting complex (RC), transition state (TS) and product complex (PC) correspond to points indicated on the plots and are provided at the top or bottom of each plot. The grey squares represent WFT reference energies, as described in the main text (DLPNO-CCSD(T)/CBS for oxo formation and NEVPT2(14,14)/def2-TZVPP for hydrogen atom transfer).

We next apply the activation strain model (ASM)¹⁵⁰⁻¹⁵², which is commonly used to rationalize reactivity trends across organic and inorganic chemistry¹⁵³⁻¹⁵⁷, to instead understand

exact exchange sensitivity along a reaction coordinate. ASM decomposes the relative energy, ΔE , at any point along a reaction coordinate into a strain component, ΔE_{str} , corresponding to the energy required to deform the reacting fragments from their equilibrium geometry to their current geometry, and an interaction component, ΔE_{int} , corresponding to the stabilization when the fragments interact at this geometry, i.e.:

$$\Delta E = \Delta E_{\text{str}} + \Delta E_{\text{int}} \quad (5)$$

where ΔE_{str} and ΔE are calculated directly and ΔE_{int} is inferred. In order to interpret exchange sensitivity in oxo formation and HAT, we define the fragments as i) the reacting small molecule (N_2O for oxo formation and CH_4 for HAT) and ii) the remainder of the complex.

For both reaction steps, ΔE_{int} is far more sensitive to exact exchange than ΔE_{str} and is the primary source of large S_i (Figure 6). This result may be expected since the ΔE_{int} for both reaction steps directly correspond to changes in the Fe BV: in oxo formation it corresponds to Fe-O bond formation, and in HAT it isolates the difference in bonding between the iron-oxo and the iron-hydroxo moieties. Thus, this ASM analysis provides further quantitative evidence that energetic sensitivity to exact exchange is driven by differences in relative Fe orbital delocalization. The evolution of the deformation density, i.e., the total electron density less the spherically symmetrized densities of isolated, constituent atoms, also provides insight into the degree of delocalized, bonding interactions (Figure 7). For oxo formation, analysis of the deformation density reveals relative depletion of Fe and O AOs with bond formation in the **TS** compared to the **RC**. In the **PC**, additional $3d$ AO depletion is observed together with even greater electron delocalization between Fe and O, consistent with prior localized orbital analysis of the equilibrium and stretched iron-oxo moieties¹³³.

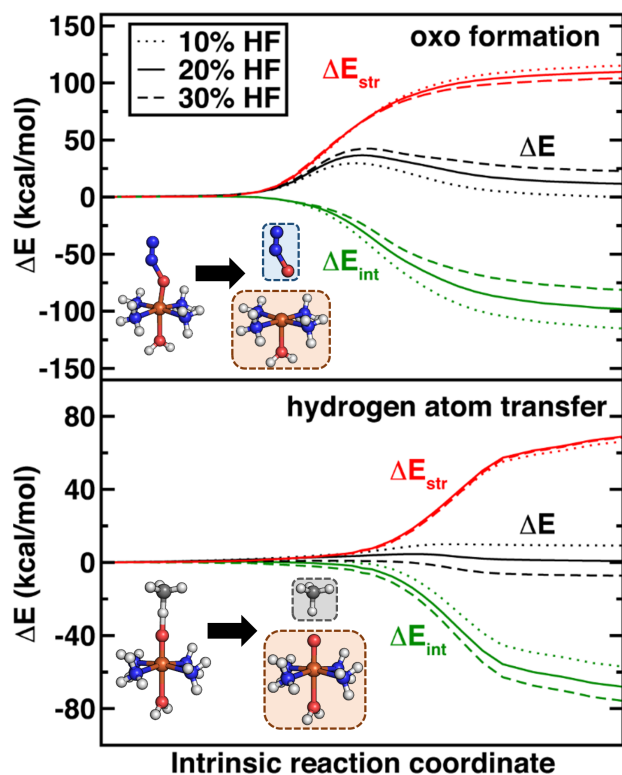


Figure 6. Activation strain model decomposed strain (ΔE_{str} , red lines) and interaction (ΔE_{int} , green lines) energy contributions to the reaction energy profiles (ΔE , black lines) at 10 (dotted lines), 20 (solid lines) and 30% (dashed lines) HF exchange for oxo formation (top) and hydrogen atom transfer (bottom). The reacting fragments are as shown in the insets. Note that the y-axis range of the oxo formation step is approximately twice that of the hydrogen atom transfer step.

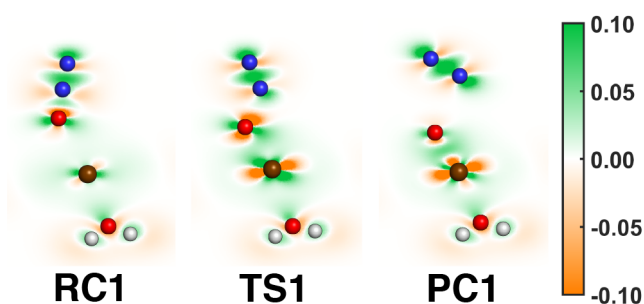


Figure 7. Illustration of the evolution of the deformation density in the oxo formation reaction step, calculated and visualized in the plane of the Fe-O-N bond. Orange and green areas represent regions of electron depletion (density loss) and electron accumulation (density gain) relative to relative to isolated atoms, respectively. Approximate atomic positions are indicated by spheres (brown: Fe, red: O, blue: N and white: H).

The ΔE_{str} contribution corresponds in oxo formation to the O-N bond dissociation and in HAT to the Fe-O stretch and C-H bond dissociation. These primarily organic bond strength

changes are less sensitive to HF exchange than the metal-ligand contributions in ΔE_{int} . For HAT, the insensitivity of ΔE_{int} to the Fe-O bond stretch is consistent with a modest Fe BV change of 0.1 and prior orbital analysis¹³³. Thus, the ASM approach enables us to approximately exclude the organic contribution (i.e., neglecting ΔE_{int}) to the overall reaction exchange sensitivity, giving corrected S_i values that quantitatively isolate the per-metal-organic-bond sensitivity. Doing so, we obtain values of 88 kcal/molbond and 119 kcal/molbond for oxo formation and HAT respectively (see Supporting Information Table S6 for details). Although small (e.g., less than 20 kcal/molHFX) sensitivity differences may be attributable to differences in linear fits²³, the significant (around 35%) difference in per-metal-organic-bond sensitivities for both reaction steps is likely a result of the differing degrees of delocalization afforded by the bonding orbitals in each case that are not distinguished by the BV metric. More delocalized Fe-O π bonds are broken in HAT, whereas a combination of π bonds and relatively localized σ bonds are formed in oxo formation (see ref. ¹³³ and Supporting Information Figure S7).

In a manner analogous to S_i , we approximate barrier height sensitivities, S_{TS} , as follows:

$$S_{\text{TS}} = \frac{\Delta(E_{\text{TS}} - E_{\text{RC}})}{\Delta a_{\text{HF}}} \approx \frac{\partial(E_{\text{TS}} - E_{\text{RC}})}{\partial a_{\text{HF}}} \quad (6)$$

where E_{TS} and E_{RC} are the energies of the **TS** and **RC**, respectively. If BV differences are greater between **RC** and **PC** than between **RC** and **TS**, we will expect S_{TS} to be smaller than S_i , depending on how late (i.e., product-like) the **TS** is. Evaluated at 20% HF exchange, S_{TS} of oxo formation and HAT are around 65 kcal/molHFX and -45 kcal/molHFX respectively, which correspond to around 55% of S_i for both reaction steps. However, it should be noted that S_{TS} of the HAT reaction step will vary strongly with HF exchange as a result of strong sensitivity of the underlying TS geometry (Figure 5, bottom). The decrease in HAT barrier with increased HF exchange, consistent with previous studies^{81, 138}, nominally violates the expectation that GGAs underestimate barrier heights⁸ due to greater delocalization in TSs than RCs. However, the 3d electrons in the HAT TS are indeed less delocalized than in the reactants, as indicated by the

lower Fe BV, and thus HAT in TM complexes corresponds to a case where penalizing delocalization (e.g., with HF exchange) should lower the barrier height.

Comparison to correlated WFT reference energetics provides some clues regarding functional choice for accurate energetics in oxo formation (grey squares in Figure 5). The triple-zeta DLPNO-CCSD(T) ΔE_{rxn} of 12 kcal/mol is in good agreement with the corresponding NEVPT2 value of 9 kcal/mol (i.e., they differ by 3 kcal/mol, or TM chemical accuracy⁹⁸), confirming that our single-reference approach is indeed reasonable for this reaction step, as observed in previous work¹⁵⁸⁻¹⁵⁹. Fortuitous error cancellation for B3LYP with a modest basis set and empirical dispersion leads to ΔE_{rxn} being underestimated by only 3 kcal/mol relative to the CBS DLPNO-CCSD(T) value. Conversely, B3LYP underestimates the oxo formation barrier by around 10 kcal/mol. Recalling that $S_{\text{rs}} < S$, we can determine that choosing a single exchange percentage to reproduce the WFT barrier will greatly worsen ΔE_{rxn} predictions, motivating instead variable exchange through an approach analogous to the variable U in the DFT+ $U(\mathbf{R})$ approach previously proposed by our group⁵⁸⁻⁵⁹.

For HAT reaction steps, spin coupling of the methyl radical and the iron-oxo species motivates MR WFT references, and B3LYP underestimates the computed NEVPT2 barrier of 11 kcal/mol by 6 kcal/mol. When paired with the S_{rs} of -45 kcal/mol HFX for HAT in this model complex, these results indicate that the B3LYP exchange fraction is too high and should be reduced to only 7% in order to reproduce the WFT barrier. Similar underestimation of HAT barriers has been observed for other nonheme Fe(IV)-oxo complexes, such as [Fe(TMC)(CH₃CN)(O)]²⁺ (TMC = 1,4,8,11-tetramethyl-1,4,8,11-tetraazacyclotetradecane)¹¹⁷ and trigonal bipyramidal Fe(NH₃)₄(O)]²⁺.¹⁶⁰ Indeed, there have been suggestions that some TM complexes are better described by functionals with reduced or no HF exchange^{65, 68, 71-72}. Divergent HF exchange dependence and optimal parameter choice along reaction coordinates and between steps in the same catalytic cycle thus motivate careful evaluation of the role of functional selection in catalyst screening studies that typically rely on a single functional. Further functional

development to produce accurate energetics across catalytic cycle would necessitate more extensive benchmarking beyond the scope of this work.

3c. Selection of Metrics to Explain Reaction Energy, Spin-Splitting, and Redox Sensitivities.

Although we have found value in the BV metric for explaining exchange sensitivities, we can try to rationalize S_r trends among catalytic steps through changes in metal-centered descriptors such as atomic partial charges and spin densities. As the HAT reaction step proceeds, spin is localized onto the Fe center and the increase in C spin density correlates well with the HF exchange sensitivity (Supporting Information Figure S6). Furthermore, the increase in exchange stabilization⁶¹ (ES) with metal spin density is a key ingredient of EER¹³⁷⁻¹³⁸, which explains why HAT barriers are lower on the quintet spin surface than on the triplet spin surface. Hence, it is plausible that S_r is similarly a result of increased ES by HF exchange⁸¹. However, this idea fails to generalize to the oxo formation reaction step, for which S_r increases monotonically but spin densities do not (Supporting Information Figure S6). Similarly, although decreases in metal partial charge from LS to HS are correlated to negative spin-splitting sensitivities^{22, 24}, the partial charges are themselves sensitive to HF exchange⁵², and they should at least weakly correspond to formal oxidation state⁶², partial charges are unsuitable as universal descriptors for S_r . This poor correlation is again evident from the oxo formation reaction step, in which the Fe partial charge decreases from 1.47 to 1.38 upon addition of the oxo group despite the large, positive S_r . Such disparity between partial charges (here, less than +2) and oxidation states (here, up to IV) is common among TM complexes¹⁶³⁻¹⁶⁴.

Having identified BV metrics as the most suitable to explain sensitivity in chemical catalysis, we return to spin-splittings to identify if the BV metric retains its transferability. For a TM complex, the LS-HS transition may be nominally defined as a unimolecular reaction:

$$\Delta E_r = \Delta E^{\text{HS-LS}} = E(\text{HS}) - E(\text{LS}) \quad (7)$$

Comparing the HF exchange sensitivity of the spin-splitting energy (denoted $S_{\text{HS-LS}}$) between bare Fe^{2+} cations, which is the limiting case of zero ligand field strength (i.e., fully degenerate $3d$ orbitals²⁴), and various Fe(II) complexes, we find that $S_{\text{HS-LS}}$ is greatly reduced in Fe^{2+} vs. the Fe(II) complexes (Supporting Information Table S7), consistent with previous observations²⁴. As localized descriptor changes are instead greater in Fe^{2+} than in Fe(II) complexes, where property changes are typically spread between the metal and ligands, this result is again inconsistent with their use as HF exchange sensitivity descriptors. Rather, as we and others have previously argued^{22, 24, 28, 52}, $S_{\text{HS-LS}}$ is primarily a result of differences in delocalization between the HS and LS states, with HF exchange favoring the HS state due to lower delocalization as a result of increased occupancy of antibonding orbitals. This difference in delocalization⁵⁹ is attenuated in weak-field complexes and completely absent in bare metal ions, leading to greatly reduced sensitivity in those cases. Hence, this failure of localized metal descriptors, both for chemical reactions and for spin state ordering, stems primarily from their inability to describe electron delocalization over the entire complex. Other descriptors for spin-splitting sensitivity, including differences in HS and LS bond lengths⁶¹, differences in HS and LS metal partial charges²², and the spin-splitting energy evaluated at 20% HF exchange (i.e., B3LYP)²², are successful because they indirectly quantify differences in electron delocalization, but these metrics are not generalizable to chemical reactions.

Thus, it is useful to identify if there is a quantitative relationship between $S_{\text{HS-LS}}$ and the change in the BV between HS and LS states. Assuming such a relationship is found, we can then compare the computed per-bond sensitivity to that previously computed for Fe(II) reactions to determine if there is any difference in sensitivity to BV changes in spin-state splitting versus catalytic energetics. To interpolate BV changes while keeping the ligand identity constant, we generated a series of $[\text{Fe}(\text{CO})_n]^{2+}$ and $[\text{Fe}(\text{NH}_3)_n]^{2+}$ complexes ($n = 1$ to 6) and compared the spin-splitting energy sensitivity and the change in BV between HS and LS states. Here, oxidation state is again constant, and therefore it cannot serve as a good predictor of relative sensitivities. Both the ammine and carbonyl complexes yielded comparable fits between sensitivity and BV

changes, with a total R^2 value of 0.97 (Figure 8). This result suggests that the suitability of the change in BV as a descriptor is independent of coordination number and bonding element identity. We then computed the spin-splitting sensitivities and BV changes for the $[\text{Fe}(\text{NH}_3)_4(\text{H}_2\text{O})(\text{O})]^{2+}$ and $[\text{Fe}(\text{imi})_3(\text{OH}_2)]^{2+}$ complexes (Sec. 3a) along with the $[\text{Fe}(\text{H}_2\text{O})_6]^{2+}$ complex. The sensitivities for these complexes are in good agreement with the computed trend (Figure 8 and Supporting Information Figure S8). The combined slope of 86 kcal/molHFXbond also matches the corrected per-bond sensitivity for oxo formation presented in Sec. 3b, further supporting the idea of a common physical origin of reaction energy and spin-splitting HF exchange sensitivities.

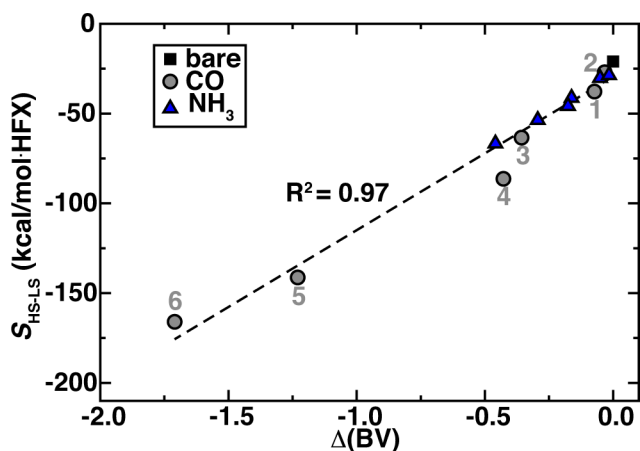


Figure 8. Spin-splitting sensitivity as a function of the difference in bond valence between HS and LS states for Fe(II) complexes of varying coordination number and ligand identity. Carbonyl and ammine complexes are denoted by gray circles and blue triangles respectively, and for comparison, the bare ion is denoted by a black square. The labels indicate the coordination number of the carbonyl complexes, and the ammine complexes follow the same ordering. All structures are relaxed at the specified spin state and coordination number, and the optimized geometries are described in Supporting Information Table S7.

As the oxo formation and HAT reaction steps are often described as redox reactions where Fe is oxidized from Fe(II) to Fe(IV) and reduced from Fe(IV) to Fe(III) respectively, we consider if S_i is related to the HF exchange sensitivity of the vertical IP (denoted S_{IP}):

$$S_{\text{IP}}(\text{X}^{n+}) = \frac{\Delta\text{IP}(\text{X}^{n+})}{\Delta a_{\text{HF}}} \approx \frac{\partial(E(\text{X}^{(n+1)+}) - E(\text{X}^{n+}))}{\partial a_{\text{HF}}} \quad (8)$$

The IPs of catalytic intermediates are often good activity descriptors¹⁶⁵⁻¹⁶⁸. In molecular catalysts, electron transfer rates in electrocatalytic reaction steps are governed directly by IPs¹⁶⁷ and chemical reactivity is dependent on frontier molecular orbital energies¹⁶⁹, which are related to IPs by Janak's theorem¹⁷⁰. Broad calculation of IP sensitivities on homoleptic octahedral complexes across the spectrochemical series revealed no clear trends with respect to ligand field strength (Supporting Information Table S8). To further probe the electronic structure factors governing S_{ip} , we systematically computed IPs for the octahedral $[\text{Fe}(\text{NH}_3)_6]^{n+}$ complex ($n = 1$ to 4) across a range of spin states, where all energies were computed at the $[\text{Fe}(\text{NH}_3)_6]^{2+}$ HS optimized geometry (Supporting Information Table S8). We found no obvious trends among S_{ip} , the ground-state electronic state, and the change in BV upon oxidation. Hence, although magnitudes of S_i and S_{ip} qualitatively agree in this system, HF exchange sensitivities of chemical catalytic steps that track with oxidation state changes are unlikely to be related to sensitivity of the underlying ionization-only reactions (Supporting Information Figure S9). Hence, in systems with simultaneous electron transfer and chemical reaction, e.g., in water-oxidation electrocatalysis¹⁶⁷, the redox and reaction sensitivities should be treated additively.

3d. Two-state Reactivity with Methane to Methanol on FeO^\bullet .

The addition-elimination reaction between FeO^\bullet and methane to form methanol is the undercoordinated Fe(III) analogue of CH_4 hydroxylation by an iron-oxo moiety. This system's differing reactivity in the accessible quartet and ground state sextet spin states, referred to as two-state reactivity (TSR)¹³⁵, has made it the focus of intense experimental¹⁷¹⁻¹⁷⁶ and computational^{56, 177-181} study. Properties of this energy landscape, including the overall reaction's exothermicity, spin inversion at the entrance and exit channel, and a shallow but excited quartet surface with respect to a steeper sextet surface, are challenging to capture within a single exchange-correlation functional. In the first step, methane binds to the diatomic cation (**Int-1**), then in the highest barrier step (**TS1**) oxygen abstracts a hydrogen (**Int-2**), and finally in the second reaction step, the methyl radical and hydroxyl combine (**TS2**) leaving a weakly bound methanol to a Fe^\bullet cation (**Int-3**) before it dissociates to form products (Figure 9). The need to simultaneously predict

spin-state ordering and reaction coordinate properties within each spin state in this reaction combine the challenges we have addressed thus far, motivating analysis of when exchange tuning can recover these features. Strong basis set sensitivity in this system necessitates special consideration (see Supporting Information).

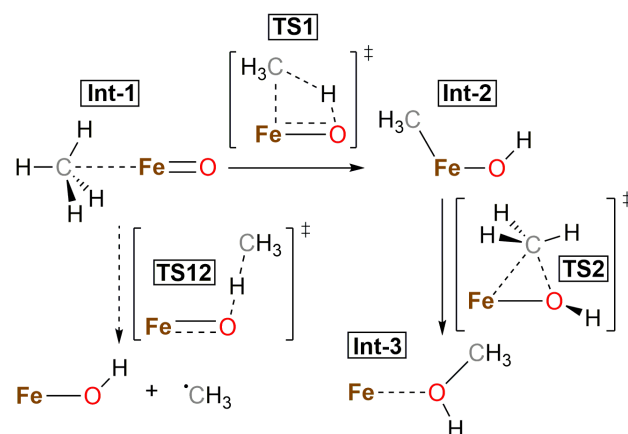


Figure 9. Key intermediates in CH_4 hydroxylation by FeO^+ . Each species has a net charge of +1 and can exist in the quartet and sextet spin states, with slight differences in geometries and bond orders between spin states.

The GGA (here, BLYP) and hybrid (here, B3LYP) energy landscapes are in qualitative agreement with prior studies^{56, 177-180} (Figure 10). The overall reaction energy, ΔE_r , is strongly sensitive to HF exchange ($S_r = -108$ kcal/molHFX on the sextet surface), consistent with the large, negative BV change (B3LYP $\Delta BV = -1.98$) due to the cleavage of the Fe-O bond when transforming from $\text{Fe}=\text{O}^+$ and CH_4 reactants to Fe^+ and CH_3OH products. On a per-bond basis, the metal-derived sensitivity after correcting for sensitivity arising from C-O bond formation (following the ASM approach described in Sec. 3b), 69 kcal/molHFXbond, is comparable to the value previously obtained for coordinated Fe(II) complexes (86 kcal/molHFXbond) (Sec. 3c). Introduction of 20% HF exchange, as in the B3LYP functional, changes the ΔE_r from erroneously endothermic with GGA to exothermic (here, -9 kcal/mol) and in good agreement with the -10 kcal/mol exothermicity observed experimentally¹⁷⁵. Continued increase of the HF exchange percentage overestimates the exothermicity of the reaction and worsens agreement with experiment.

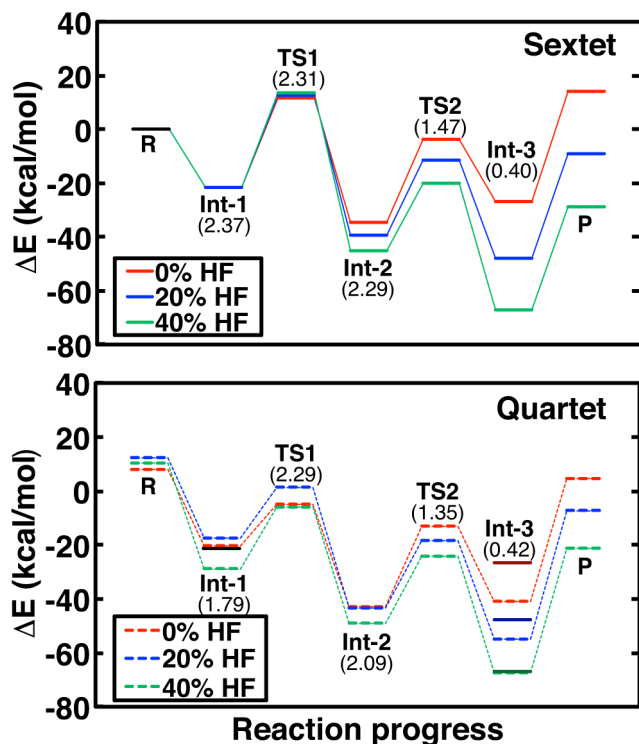


Figure 10. Energy level diagram for the FeO^+/CH_4 reaction computed at 0% (red), 20% (blue) and 40% (green) HF exchange. Solid and dotted lines represent the sextet and quartet surfaces respectively, and all energies are reported relative to the energy of ${}^6\text{FeO}^+/\text{CH}_4$ at each value of HF exchange. The labels below each species indicate the Fe bond valence computed at 20% HF exchange. The darker-colored lines at the entrance and exit channels in the quartet subplot indicate the respective sextet values for easy comparison of spin-splittings. As discussed in the main text, ${}^6\text{TS1}$ and ${}^4\text{TS1}$ could not be located at 40% HF exchange, and extrapolated values are instead shown for illustrative purposes. A combined sextet/quartet energy level diagram at 20% HF exchange is provided in Supporting Information Figure S10.

Reviewing sensitivity of individual intermediates in these reaction steps reveals some counterintuitive but easily rationalized behavior of HF exchange. At the entrance channel intermediate, ${}^4\text{Int-1}$ is correctly predicted to be more stable than ${}^6\text{Int-1}$ at low to moderate HF exchange values (< 30% HF exchange), but spin crossover occurs at about 30% HF exchange making ${}^6\text{Int-1}$ instead more stable. The stabilization of a state with lower spin multiplicity by HF exchange is contrary to typical observations in TM complexes that HF exchange favors high-spin states^{22, 61, 74}, but this effect is consistent with our attribution of HF exchange sensitivity to differences in metal-ligand delocalization. The stronger Fe-O bonding in ${}^6\text{Int-1}$ than in ${}^4\text{Int-1}$, as evidenced by the Fe-O bond order, is penalized with increasing HF exchange (Figure 10).

Approximate agreement of the ${}^4\text{Int-1}/{}^4\text{Int-1}$ splitting ($\Delta E^{\text{HS-LS}} = -8$ kcal/mol) and ${}^4\text{Int-1}/\text{TS12}$ barrier ($E_s = 12$ kcal/mol) with MR WFT reference energies⁵⁶ is achieved at low (i.e., 10%) HF exchange.

In contrast to the low exchange favored at the entrance channel, the ground state of the exit channel (i.e., **Int-3**) is incorrectly predicted to be the quartet for HF exchange values of less than about 40%. The B3LYP (i.e., 20% exchange) splitting of 7 kcal/mol overestimates the WFT reference of -3 kcal/mol⁵⁶ by about 10 kcal/mol, which is further exacerbated by the low sensitivity of this intermediate to HF exchange ($S_{\text{HS-LS}} = -35$ kcal/molHFX) that arises from an almost unchanged, relatively low Fe-O bond order for both quartet and sextet states. Very high exchange fractions (i.e., about 50%) are required to achieve quantitative agreement with the WFT reference splitting energy for these two intermediates. It is noteworthy that B3LYP with the same basis set predicts the spin-state splitting of the bare Fe⁺ ion (the final reaction product) to within TM chemical accuracy (i.e., an absolute error of 3 kcal/mol relative to the experimental value¹⁸²), which suggests an unusually large effect of weak ligand field perturbation on DFT spin-splitting errors.

Across extended (i.e., 0-40%) ranges of HF exchange, we observe strong nonlinearity in the effect of HF exchange on the quartet energy landscape, particularly in the relative energies of **Int-1** and **Int-2** (Figure 10). We have treated HF sensitivities as approximately constant over moderate ranges of HF exchange, which has been a good assumption thus far, although some nonlinearity at high exchange fractions has been noted in prior work²¹⁻²². We can account for deviations from linearity in terms of shifts of the underlying BV changes with HF exchange:

$$\frac{\partial^2 \Delta E_r}{\partial a_{\text{HF}}^2} = \frac{\partial S_r}{\partial a_{\text{HF}}} \propto \frac{\partial \Delta(\text{BV})}{\partial a_{\text{HF}}} \quad (9)$$

Strong deviations from linearity typically from qualitative changes in hybridization of either of the two states being compared with HF exchange. Here, ${}^4\text{FeO}^+$ undergoes a marked increase in spin-up 3d density of π^* orbitals coupled with a reduction of the partial 3d occupation in spin-

down π orbitals^{19, 56}, which results in a 0.8 decrease in the Fe-O bond order from 0 to 40% HF exchange. The imbalance in spin-up and spin-down density changes also leads to a 1.0 e increase in the Fe Löwdin spin density. In contrast, the Fe-O bond order and Fe spin density in ${}^4\text{FeO}$ decrease only by 0.3 bond and 0.1 e respectively over the same range of HF exchange. Caution is thus warranted when identifying and interpreting trends over extended ranges of HF exchange as the qualitative electronic state may vary in the low and high HF exchange limits.

Although high exchange is recommended for some portions of the reaction coordinate, use of large exchange fractions can alter mechanistic predictions. At 30 and 40% HF exchange, the concerted **TS1** could not be located for either the sextet or quartet surfaces, likely because the potential energy surface is perturbed sufficiently by the destabilization of Fe-C bonding that no saddle point exists along the reaction coordinate, and TS searches instead yield the direct **TS12** that corresponds to a HAT reaction step¹⁸¹ analogous to that studied in Secs. 3a and 3b. Concomitant relative stabilization of the direct **TS12** over the concerted **TS1** with increasing HF exchange should also lead to lower predicted CH_3OH yields, as the direct **TS12** favors dissociation of the methyl radical over formation of **Int-2**. Nevertheless, extrapolating barrier heights based on sensitivities derived from 0 to 20% HF exchange, the quartet surface remains more reactive than the sextet surface for a wide range of HF exchange values, as the destabilization of ${}^4\text{TS1}$ relative to ${}^6\text{TS1}$ is balanced by stabilization of ${}^4\text{Int-1}$ over ${}^6\text{Int-1}$ (Figure 10).

The preceding analysis further demonstrates that inherent imbalances in GGA errors and sensitivities lead to substantial variability in optimal parameter choice over the entire energy landscape, ranging from 10% at the entrance channel, 20% for the overall reaction to about 50% HF exchange at the exit channel. Compared to studies on more saturated complexes, the variations here are more pronounced as very weak coordination in the exit channel yields lower sensitivities for spin-state splittings. In this light, comparison to a DFT+U study by Kulik *et al.*⁵⁶, in which a global-average of self-consistent calculated values of U at 5 eV was used to improve GGA (PBE in that work) predictions across the entire energy landscape, is instructive. The

DFT+U approach is essentially an explicit energetic penalization of hybridized metal-ligand bonding orbitals with fractional metal 3d character relative to nonbonding states³⁶, an effect which has motivated our study into how BV metrics rationalize HF exchange tuning of reaction energetics. Indeed, the qualitative effects of exact exchange and the +U correction on geometric and energetic trends in this system are the same, with only slight differences (e.g., more weakly bound ⁶TS2 geometries and the failure to converge metastable nonplanar ⁴Int-1 geometries) that may be attributed to differences in GGA functional (PBE vs. BLYP) or basis set formalism (plane-wave vs. atom-centered). Comparison of sensitivities of reaction and spin-splitting energies to HF exchange and U yielded qualitative agreement as well (Supporting Information Figure S11). With DFT+U as with HF exchange, although a global single parameter is typically used to make total energies comparable, variations in optimal exchange fraction or U value also motivate strategies⁵⁸⁻⁵⁹ to explicitly incorporate those variations into reaction pathway analysis, and such work is ongoing in our group.

4. Conclusions

Through a careful study of several model complexes, we have computed reaction barriers and energetics for model open-shell iron catalysts to have comparable exact exchange sensitivity to the large sensitivities of adiabatic spin-state splittings. This analysis has led us to rationalize high exchange sensitivities through transferable and simple-to-compute change in BV that now unifies explanations for exchange sensitivity of catalytic properties and spin-state ordering in transition metal complexes.

Within model catalytic cycles involving both open-shell (i.e., Fe(II)) and closed-shell (i.e., Zn(II)) transition metal centers, we rationalized differences in exchange sensitivity between catalytic steps, as well as continuous evolution of sensitivity along reaction coordinates, in terms of BV changes. In the case of methane hydroxylation by a Fe(II) model biomimetic complex: i) strong HF exchange dependence of the computed TOF and ii) divergent HF exchange dependence and optimal parameter choice along continuous evaluation of the reaction coordinates and between steps motivate careful evaluation of the role of functional selection in

catalyst screening studies.

Over a range of ligand field strengths and coordination numbers, we confirmed a strong correspondence between the sensitivities of spin-splitting energies of representative Fe(II) complexes to HF exchange and the change in BV between the high- and low-spin states. Close agreement of the resulting per-metal-organic-bond sensitivity estimate with those obtained for energetics of catalytic steps, together with failure of alternative descriptors, demonstrates that the BV is a robust and transferable descriptor of how differences in metal-ligand delocalization produce differing relative energetics with exchange tuning. Future study of a wider range of energetics, e.g., vertical ionization potentials, or reactions with other complex types, e.g., closed shell TM centers, may motivate extensions to the BV metric.

To illustrate the utility of our unified approach, we studied the effect of HF exchange tuning on a system that combines both spin-state considerations and chemical catalysis, namely the paradigmatic TSR addition-elimination reaction between FeO[•] and methane. Here, trends in barrier heights, reaction energies and spin-splitting energies with varying HF exchange were again consistent with BV differences. The availability of accurate experimental and WFT references enabled us to identify pronounced variability in optimal parameter choice (~10 to 50% HF exchange) over the entire energy landscape. This variation could be attributed to low spin-state splitting sensitivity in the exit channel arising from weak coordination but relatively high-sensitivity of the entrance channel, consistent with earlier observations of the manner in which DFT+U penalties on hybridized metal-ligand bonding orbitals shifted reaction energetics for this system. Overall, these observations motivate and inform the development of more flexible methods for catalyst screening beyond single hybrid functionals, and such efforts are underway within our group.

ASSOCIATED CONTENT

Supporting Information. Coordinates of optimized geometries; list of absolute energies, key distances and BVs; additional computational details for Sec. 3d; representative basis set

sensitivities; effect of D3 correction; list of complexes studied; comparison of maximum PNO amplitudes and BV changes; comparison of BV metrics; comparison of vibrational frequencies across exact exchange fractions; Gibbs energy sensitivity correlation; spin-state splittings of Fe(II)(imi)₃(H₂O); comparison of bonding in model Fe(II) and Zn(II) complexes; comparison of sensitivity descriptors across reaction coordinates; calculation of per-metal-organic-bond sensitivities; bonding changes in hydrogen atom transfer; comparison of spin-splitting sensitivities across ions and complexes; additional spin-splitting sensitivities and BV changes; selected vertical IPs; comparison of selected reaction energy and vertical IP sensitivities; comparison of HF exchange and U sensitivities of FeO⁺/CH₄ steps; combined B3LYP ⁶⁴FeO⁺/CH₄ energy level diagram. This material is available free of charge via the Internet at <http://pubs.acs.org>.

AUTHOR INFORMATION

Corresponding Author

*email: hjkulik@mit.edu phone: 617-253-4584

Notes

The authors declare no competing financial interest.

ACKNOWLEDGMENT

This work was supported in part by the National Science Foundation under grant number CBET-1704266. H.J.K. holds a Career Award at the Scientific Interface from the Burroughs Wellcome Fund. This work was carried out in part using computational resources from the Extreme Science and Engineering Discovery Environment (XSEDE), which is supported by National Science Foundation grant number ACI-1053575. The authors thank Adam H. Steeves for providing a critical reading of the manuscript.

REFERENCES

1. Vogiatzis, K. D.; Haldoupis, E.; Xiao, D. J.; Long, J. R.; Siepmann, J. I.; Gagliardi, L., Accelerated Computational Analysis of Metal–Organic Frameworks for Oxidation Catalysis. *J. Phys. Chem. C* **2016**, *120*, 18707-18712.

2. Bernales, V.; League, A. B.; Li, Z.; Schweitzer, N. M.; Peters, A. W.; Carlson, R. K.; Hupp, J. T.; Cramer, C. J.; Farha, O. K.; Gagliardi, L., Computationally Guided Discovery of a Catalytic Cobalt-Decorated Metal–Organic Framework for Ethylene Dimerization. *J. Phys. Chem. C* **2016**, *120*, 23576-23583.
3. Pahls, D. R.; Ortuño, M. A.; Winegar, P. H.; Cramer, C. J.; Gagliardi, L., Computational Screening of Bimetal-Functionalized Zr₆O₈ Mof Nodes for Methane C–H Bond Activation. *Inorg. Chem.* **2017**, *56*, 8739-8743.
4. Krausbeck, F.; Sobez, J. G.; Reiher, M., Stabilization of Activated Fragments by Shell-Wise Construction of an Embedding Environment. *J. Comput. Chem.* **2017**, *38*, 1023-1038.
5. Mori-Sánchez, P.; Cohen, A. J.; Yang, W., Many-Electron Self-Interaction Error in Approximate Density Functionals. *J. Chem. Phys.* **2006**, *125*, 201102.
6. Ruzsinszky, A.; Perdew, J. P.; Csonka, G. I.; Vydrov, O. A.; Scuseria, G. E., Density Functionals That Are One- and Two- Are Not Always Many-Electron Self-Interaction-Free, as Shown for H₂⁺, He₂⁺, LiH⁺, and Ne₂⁺. *J. Chem. Phys.* **2007**, *126*, 104102.
7. Haunschild, R.; Henderson, T. M.; Jiménez-Hoyos, C. A.; Scuseria, G. E., Many-Electron Self-Interaction and Spin Polarization Errors in Local Hybrid Density Functionals. *J. Chem. Phys.* **2010**, *133*, 134116.
8. Cohen, A. J.; Mori-Sánchez, P.; Yang, W., Insights into Current Limitations of Density Functional Theory. *Science* **2008**, *321*, 792-794.
9. Schmidt, T.; Kümmel, S., One- and Many-Electron Self-Interaction Error in Local and Global Hybrid Functionals. *Phys. Rev. B* **2016**, *93*, 165120.
10. Kim, M.-C.; Sim, E.; Burke, K., Understanding and Reducing Errors in Density Functional Calculations. *Phys. Rev. Lett.* **2013**, *111*, 073003.
11. Zheng, X.; Liu, M.; Johnson, E. R.; Contreras-García, J.; Yang, W., Delocalization Error of Density-Functional Approximations: A Distinct Manifestation in Hydrogen Molecular Chains. *J. Chem. Phys.* **2012**, *137*, 214106.
12. Johnson, E. R.; Otero-de-la-Roza, A.; Dale, S. G., Extreme Density-Driven Delocalization Error for a Model Solvated-Electron System. *J. Chem. Phys.* **2013**, *139*, 184116.
13. Cramer, C. J.; Truhlar, D. G., Density Functional Theory for Transition Metals and Transition Metal Chemistry. *Phys. Chem. Chem. Phys.* **2009**, *11*, 10757-10816.
14. Ruzsinszky, A.; Perdew, J. P.; Csonka, G. I.; Vydrov, O. A.; Scuseria, G. E., Spurious Fractional Charge on Dissociated Atoms: Pervasive and Resilient Self-Interaction Error of Common Density Functionals. *J. Chem. Phys.* **2006**, *125*, 194112.
15. Dutoi, A. D.; Head-Gordon, M., Self-Interaction Error of Local Density Functionals for Alkali–Halide Dissociation. *Chem. Phys. Lett.* **2006**, *422*, 230-233.
16. Bally, T.; Sastry, G. N., Incorrect Dissociation Behavior of Radical Ions in Density Functional Calculations. *J. Phys. Chem. A* **1997**, *101*, 7923-7925.
17. Zhang, Y.; Yang, W., A Challenge for Density Functionals: Self-Interaction Error Increases for Systems with a Noninteger Number of Electrons. *J. Chem. Phys.* **1998**, *109*, 2604-2608.
18. Johnson, B. G.; Gonzales, C. A.; Gill, P. M. W.; Pople, J. A., A Density Functional Study of the Simplest Hydrogen Abstraction Reaction. Effect of Self-Interaction Correction. *Chem. Phys. Lett.* **1994**, *221*, 100-108.
19. Kulik, H. J.; Cococcioni, M.; Scherlis, D. A.; Marzari, N., Density Functional Theory in Transition-Metal Chemistry: A Self-Consistent Hubbard U Approach. *Phys. Rev. Lett.* **2006**, *97*, 103001.
20. Ganzenmüller, G.; Berkaine, N.; Fouqueau, A.; Casida, M. E.; Reiher, M., Comparison of Density Functionals for Differences between the High- (T_{2g}⁵) and Low- (A_{1g}¹) Spin States of Iron(II) Compounds. IV. Results for the Ferrous Complexes [Fe(L)(‘NHS₄’)]. *J. Chem. Phys.* **2005**, *122*, 234321.
21. Droghetti, A.; Alfè, D.; Sanvito, S., Assessment of Density Functional Theory for Iron (II) Molecules across the Spin-Crossover Transition. *J. Chem. Phys.* **2012**, *137*, 124303.

22. Ioannidis, E. I.; Kulik, H. J., Towards Quantifying the Role of Exact Exchange in Predictions of Transition Metal Complex Properties. *J. Chem. Phys.* **2015**, *143*, 034104.
23. Mortensen, S. R.; Kepp, K. P., Spin Propensities of Octahedral Complexes from Density Functional Theory. *J. Phys. Chem. A* **2015**, *119*, 4041-4050.
24. Ioannidis, E. I.; Kulik, H. J., Ligand-Field-Dependent Behavior of Meta-GGA Exchange in Transition-Metal Complex Spin-State Ordering. *J. Phys. Chem. A* **2017**, *121*, 874-884.
25. Autschbach, J.; Srebro, M., Delocalization Error and “Functional Tuning” in Kohn–Sham Calculations of Molecular Properties. *Acc. Chem. Res.* **2014**, *47*, 2592-2602.
26. Kulik, H. J., Perspective: Treating Electron over-Delocalization with the DFT+U Method. *J. Chem. Phys.* **2015**, *142*, 240901.
27. Janet, J. P.; Zhao, Q.; Ioannidis, E. I.; Kulik, H. J., Density Functional Theory for Modelling Large Molecular Adsorbate–Surface Interactions: A Mini-Review and Worked Example. *Mol. Simul.* **2017**, *43*, 327-345.
28. Wilbraham, L.; Verma, P.; Truhlar, D. G.; Gagliardi, L.; Ciofini, I., Multiconfiguration Pair-Density Functional Theory Predicts Spin-State Ordering in Iron Complexes with the Same Accuracy as Complete Active Space Second-Order Perturbation Theory at a Significantly Reduced Computational Cost. *J. Phys. Chem. Lett.* **2017**, *8*, 2026-2030.
29. Perdew, J. P.; Parr, R. G.; Levy, M.; Balduz, J. L., Density-Functional Theory for Fractional Particle Number: Derivative Discontinuities of the Energy. *Phys. Rev. Lett.* **1982**, *49*, 1691-1694.
30. Vydrov, O. A.; Scuseria, G. E.; Perdew, J. P., Tests of Functionals for Systems with Fractional Electron Number. *J. Chem. Phys.* **2007**, *126*, 154109.
31. Yang, W.; Zhang, Y.; Ayers, P. W., Degenerate Ground States and a Fractional Number of Electrons in Density and Reduced Density Matrix Functional Theory. *Phys. Rev. Lett.* **2000**, *84*, 5172-5175.
32. Perdew, J. P.; Levy, M., Physical Content of the Exact Kohn-Sham Orbital Energies: Band Gaps and Derivative Discontinuities. *Phys. Rev. Lett.* **1983**, *51*, 1884-1887.
33. Sham, L. J.; Schlüter, M., Density-Functional Theory of the Energy Gap. *Phys. Rev. Lett.* **1983**, *51*, 1888-1891.
34. Sagvolden, E.; Perdew, J. P., Discontinuity of the Exchange-Correlation Potential: Support for Assumptions Used to Find It. *Phys. Rev. A* **2008**, *77*, 012517.
35. Mori-Sanchez, P.; Cohen, A. J., The Derivative Discontinuity of the Exchange-Correlation Functional. *Phys. Chem. Chem. Phys.* **2014**, *16*, 14378-14387.
36. Leininger, T.; Stoll, H.; Werner, H.-J.; Savin, A., Combining Long-Range Configuration Interaction with Short-Range Density Functionals. *Chem. Phys. Lett.* **1997**, *275*, 151-160.
37. Iikura, H.; Tsuneda, T.; Yanai, T.; Hirao, K., A Long-Range Correction Scheme for Generalized-Gradient-Approximation Exchange Functionals. *J. Chem. Phys.* **2001**, *115*, 3540-3544.
38. Toulouse, J.; Colonna, F.; Savin, A., Long-Range-Short-Range Separation of the Electron–Electron Interaction in Density-Functional Theory. *Phys. Rev. A* **2004**, *70*, 062505.
39. Baer, R.; Neuhauser, D., Density Functional Theory with Correct Long-Range Asymptotic Behavior. *Phys. Rev. Lett.* **2005**, *94*, 043002.
40. Vydrov, O. A.; Scuseria, G. E., Assessment of a Long-Range Corrected Hybrid Functional. *J. Chem. Phys.* **2006**, *125*, 234109.
41. Livshits, E.; Baer, R., A Well-Tempered Density Functional Theory of Electrons in Molecules. *Phys. Chem. Chem. Phys.* **2007**, *9*, 2932-2941.
42. Cohen, A. J.; Mori-Sánchez, P.; Yang, W., Development of Exchange-Correlation Functionals with Minimal Many-Electron Self-Interaction Error. *J. Chem. Phys.* **2007**, *126*, 191109.
43. Salzner, U.; Baer, R., Koopmans’ Springs to Life. *J. Chem. Phys.* **2009**, *131*, 231101.
44. Tsuneda, T.; Song, J.-W.; Suzuki, S.; Hirao, K., On Koopmans’ Theorem in Density Functional Theory. *J. Chem. Phys.* **2010**, *133*, 174101.

45. Srebro, M.; Autschbach, J., Does a Molecule-Specific Density Functional Give an Accurate Electron Density? The Challenging Case of the CuCl Electric Field Gradient. *J. Phys. Chem. Lett.* **2012**, *3*, 576-581.
46. Anisimov, V. I.; Zaanen, J.; Andersen, O. K., Band Theory and Mott Insulators - Hubbard-U Instead of Stoner-I. *Phys. Rev. B* **1991**, *44*, 943-954.
47. Liechtenstein, A. I.; Anisimov, V. I.; Zaanen, J., Density-Functional Theory and Strong-Interactions - Orbital Ordering in Mott-Hubbard Insulators. *Phys. Rev. B* **1995**, *52*, R5467-R5470.
48. Dudarev, S. L.; Botton, G. A.; Savrasov, S. Y.; Humphreys, C. J.; Sutton, A. P., Electron-Energy-Loss Spectra and the Structural Stability of Nickel Oxide: An LSDA+U Study. *Phys. Rev. B* **1998**, *57*, 1505-1509.
49. Zunger, A.; Freeman, A. J., Ground- and Excited-State Properties of LiF in the Local-Density Formalism. *Phys. Rev. B* **1977**, *16*, 2901-2926.
50. Pederson, M. R.; Heaton, R. A.; Lin, C. C., Density-Functional Theory with Self-Interaction Correction: Application to the Lithium Molecule. *J. Chem. Phys.* **1985**, *82*, 2688-2699.
51. Pederson, M. R.; Ruzsinszky, A.; Perdew, J. P., Communication: Self-Interaction Correction with Unitary Invariance in Density Functional Theory. *J. Chem. Phys.* **2014**, *140*, 121103.
52. Gani, T. Z. H.; Kulik, H. J., Where Does the Density Localize? Convergent Behavior for Global Hybrids, Range Separation, and DFT+U. *J. Chem. Theory Comput.* **2016**.
53. Pritchard, B.; Autschbach, J., Theoretical Investigation of Paramagnetic NMR Shifts in Transition Metal Acetylacetonato Complexes: Analysis of Signs, Magnitudes, and the Role of the Covalency of Ligand-Metal Bonding. *Inorg. Chem.* **2012**, *51*, 8340-8351.
54. Duignan, T.; Autschbach, J., Impact of the Kohn-Sham Delocalization Error on the 4f Shell Localization and Population in Lanthanide Complexes. *J. Chem. Theory Comput.* **2016**.
55. Duignan, T.; Autschbach, J.; Batista, E.; Yang, P., Assessment of Tuned Range Separated Exchange Functionals for Spectroscopies and Properties of Uranium Complexes. *J. Chem. Theory Comput.* **2017**.
56. Kulik, H. J.; Marzari, N., A Self-Consistent Hubbard U Density-Functional Theory Approach to the Addition-Elimination Reactions of Hydrocarbons on Bare FeO+. *J. Chem. Phys.* **2008**, *129*, 134314.
57. Mosey, N. J.; Liao, P.; Carter, E. A., Rotationally Invariant Ab Initio Evaluation of Coulomb and Exchange Parameters for DFT+ U Calculations. *J. Chem. Phys.* **2008**, *129*, 014103.
58. Kulik, H. J.; Marzari, N., Accurate Potential Energy Surfaces with a DFT+U(R) Approach. *J. Chem. Phys.* **2011**, *135*, 194105.
59. Zhao, Q.; Ioannidis, E. I.; Kulik, H. J., Global and Local Curvature in Density Functional Theory. *J. Chem. Phys.* **2016**, *145*, 054109.
60. Kümmel, S.; Kronik, L., Orbital-Dependent Density Functionals: Theory and Applications. *Rev. Mod. Phys.* **2008**, *80*, 3-60.
61. Bowman, D. N.; Jakubikova, E., Low-Spin Versus High-Spin Ground State in Pseudo-Octahedral Iron Complexes. *Inorg. Chem.* **2012**, *51*, 6011-6019.
62. Smith, D. M.; Dupuis, M.; Straatsma, T., Multiplet Splittings and Other Properties from Density Functional Theory: An Assessment in Iron-Porphyrin Systems. *Mol. Phys.* **2005**, *103*, 273-278.
63. Bruschi, M.; De Gioia, L.; Zampella, G.; Reiher, M.; Fantucci, P.; Stein, M., A Theoretical Study of Spin States in Ni-S4 Complexes and Models of the [Nife] Hydrogenase Active Site. *J. Biol. Inorg. Chem.* **2004**, *9*, 873-884.
64. Verma, P.; Varga, Z.; Klein, J. E.; Cramer, C. J.; Que, L.; Truhlar, D. G., Assessment of Electronic Structure Methods for the Determination of the Ground Spin States of Fe (Ii), Fe (Iii) and Fe (Iv) Complexes. *Phys. Chem. Chem. Phys.* **2017**, *19*, 13049-13069.
65. Kepp, K. P., Consistent Descriptions of Metal-Ligand Bonds and Spin-Crossover in Inorganic Chemistry. *Coord. Chem. Rev.* **2013**, *257*, 196-209.

66. Huang, W.; Xing, D.-H.; Lu, J.-B.; Long, B.; Schwarz, W. E.; Li, J., How Much Can Density Functional Approximations (DFA) Fail? The Extreme Case of the FeO₄ Species. *J. Chem. Theory Comput.* **2016**, *12*, 1525-1533.
67. Jensen, K. P.; Ryde, U., Theoretical Prediction of the Co– C Bond Strength in Cobalamins. *J. Phys. Chem. A* **2003**, *107*, 7539-7545.
68. Jensen, K. P.; Roos, B. O.; Ryde, U., Performance of Density Functionals for First Row Transition Metal Systems. *J. Chem. Phys.* **2007**, *126*, 014103.
69. Jensen, K. P., Bioinorganic Chemistry Modeled with the TPSSh Density Functional. *Inorg. Chem.* **2008**, *47*, 10357-10365.
70. Jensen, K. P., Metal– Ligand Bonds of Second-and Third-Row d-Block Metals Characterized by Density Functional Theory. *J. Phys. Chem. A* **2009**, *113*, 10133-10141.
71. Furche, F.; Perdew, J. P., The Performance of Semilocal and Hybrid Density Functionals in 3 d Transition-Metal Chemistry. *J. Chem. Phys.* **2006**, *124*, 044103.
72. Perdew, J. P.; Ernzerhof, M.; Burke, K., Rationale for Mixing Exact Exchange with Density Functional Approximations. *J. Chem. Phys.* **1996**, *105*, 9982-9985.
73. Weymuth, T.; Couzijn, E. P.; Chen, P.; Reiher, M., New Benchmark Set of Transition-Metal Coordination Reactions for the Assessment of Density Functionals. *J. Chem. Theory Comput.* **2014**, *10*, 3092-3103.
74. Reiher, M.; Salomon, O.; Hess, B. A., Reparameterization of Hybrid Functionals Based on Energy Differences of States of Different Multiplicity. *Theor. Chem. Acc.* **2001**, *107*, 48-55.
75. Reiher, M., Theoretical Study of the Fe (Phen) 2 (NCS) 2 Spin-Crossover Complex with Reparametrized Density Functionals. *Inorg. Chem.* **2002**, *41*, 6928-6935.
76. Fouqueau, A.; Mer, S.; Casida, M. E.; Lawson Daku, L. M.; Hauser, A.; Mineva, T.; Neese, F., Comparison of Density Functionals for Energy and Structural Differences between the High- [5t2g:(T2g)4(Eg)2] and Low- [1a1g:(T2g)6(Eg)0] Spin States of the Hexaquoferrous Cation [Fe(H₂O)6]2+. *J. Chem. Phys.* **2004**, *120*, 9473-9486.
77. Fouqueau, A.; Casida, M. E.; Lawson Daku, L. M. H., Andreas; Neese, F., Comparison of Density Functionals for Energy and Structural Differences between the High-[5t2g:(T2g) 4 (Eg) 2] and Low-[1a1g:(T2g) 6 (Eg) 0] Spin States of Iron (II) Coordination Compounds. II. More Functionals and the Hexaminoferrous Cation,[Fe (NH₃) 6] 2+. *J. Chem. Phys.* **2005**, *122*, 044110.
78. Salomon, O.; Reiher, M.; Hess, B. A., Assertion and Validation of the Performance of the B3LYP* Functional for the First Transition Metal Row and the G2 Test Set. *J. Chem. Phys.* **2002**, *117*, 4729-4737.
79. Isley III, W. C.; Zarra, S.; Carlson, R. K.; Bilbeisi, R. A.; Ronson, T. K.; Nitschke, J. R.; Gagliardi, L.; Cramer, C. J., Predicting Paramagnetic 1 H NMR Chemical Shifts and State-Energy Separations in Spin-Crossover Host–Guest Systems. *Phys. Chem. Chem. Phys.* **2014**, *16*, 10620-10628.
80. Janet, J. P.; Kulik, H. J., Predicting Electronic Structure Properties of Transition Metal Complexes with Neural Networks. *Chem. Sci.* **2017**, *8*, 5137-5152.
81. Johansson, A. J.; Blomberg, M. R. A.; Siegbahn, P. E. M., Quantum Chemical Modeling of the Oxidation of Dihydroanthracene by the Biomimetic Nonheme Iron Catalyst [(Tmc) Feiv (O)] 2+. *J. Phys. Chem. C* **2007**, *111*, 12397-12406.
82. Johansson, A. J.; Blomberg, M. R. A.; Siegbahn, P. E. M., Quantifying the Effects of the Self-Interaction Error in Density Functional Theory: When Do the Delocalized States Appear? II. Iron-Oxo Complexes and Closed-Shell Substrate Molecules. *J. Chem. Phys.* **2008**, *129*, 154301.
83. Wójcik, A.; Radon, M.; Borowski, T., Mechanism of O₂ Activation by A-Ketoglutarate Dependent Oxygenases Revisited. A Quantum Chemical Study. *J. Phys. Chem. A* **2016**, *120*, 1261-1274.
84. Sutton, J. E.; Guo, W.; Katsoulakis, M. A.; Vlachos, D. G., Effects of Correlated Parameters and Uncertainty in Electronic-Structure-Based Chemical Kinetic Modelling. *Nat. Chem.* **2016**, *8*, 331-337.

85. Walker, E.; Ammal, S. C.; Terejanu, G. A.; Heyden, A., Uncertainty Quantification Framework Applied to the Water–Gas Shift Reaction over Pt-Based Catalysts. *J. Phys. Chem. C* **2016**, *120*, 10328-10339.
86. Simm, G. N.; Reiher, M., Systematic Error Estimation for Chemical Reaction Energies. *J. Chem. Theory Comput.* **2016**, *12*, 2762-2773.
87. Petachem. <http://www.petachem.com>. (accessed June 01, 2017).
88. Ufimtsev, I. S.; Martinez, T. J., Quantum Chemistry on Graphical Processing Units. 3. Analytical Energy Gradients, Geometry Optimization, and First Principles Molecular Dynamics. *J. Chem. Theory Comput.* **2009**, *5*, 2619-2628.
89. Hay, P. J.; Wadt, W. R., Ab Initio Effective Core Potentials for Molecular Calculations. Potentials for the Transition Metal Atoms Sc to Hg. *J. Chem. Phys.* **1985**, *82*, 270-283.
90. Wadt, W. R.; Hay, P. J., Ab Initio Effective Core Potentials for Molecular Calculations. Potentials for Main Group Elements Na to Bi. *J. Chem. Phys.* **1985**, *82*, 284-298.
91. Janet, J. P.; Gani, T. Z. H.; Steeves, A. H.; Ioannidis, E. I.; Kulik, H. J., Leveraging Cheminformatics Strategies for Inorganic Discovery: Application to Redox Potential Design. *Ind. Eng. Chem. Res.* **2017**, *56*, 4898-4910.
92. Becke, A. D., Density-Functional Thermochemistry. III. The Role of Exact Exchange. *J. Chem. Phys.* **1993**, *98*, 5648-5652.
93. Lee, C.; Yang, W.; Parr, R. G., Development of the Colle-Salvetti Correlation-Energy Formula into a Functional of the Electron Density. *Phys. Rev. B* **1988**, *37*, 785-789.
94. Stephens, P. J.; Devlin, F. J.; Chabalowski, C. F.; Frisch, M. J., Ab Initio Calculation of Vibrational Absorption and Circular Dichroism Spectra Using Density Functional Force Fields. *J. Phys. Chem.* **1994**, *98*, 11623-11627.
95. Grimme, S.; Antony, J.; Ehrlich, S.; Krieg, H., A Consistent and Accurate Ab Initio Parametrization of Density Functional Dispersion Correction (DFT-D) for the 94 Elements H-Pu. *J. Chem. Phys.* **2010**, *132*, 154104.
96. Vosko, S. H.; Wilk, L.; Nusair, M., Accurate Spin-Dependent Electron Liquid Correlation Energies for Local Spin-Density Calculations - a Critical Analysis. *Can. J. Phys.* **1980**, *58*, 1200-1211.
97. Grimme, S.; Ehrlich, S.; Goerigk, L., Effect of the Damping Function in Dispersion Corrected Density Functional Theory. *J. Comput. Chem.* **2011**, *32*, 1456-1465.
98. Jiang, W.; DeYonker, N. J.; Determan, J. J.; Wilson, A. K., Toward Accurate Theoretical Thermochemistry of First Row Transition Metal Complexes. *J. Phys. Chem. A* **2011**, *116*, 870-885.
99. Swart, M.; Bickelhaupt, F. M.; Duran, M. Popularity Poll of DFT Functionals. <http://www.marcelswart.eu/dft-poll/> (accessed July 22, 2017).
100. Wang, L.-P.; Song, C., Geometry Optimization Made Simple with Translation and Rotation Coordinates. *J. Chem. Phys.* **2016**, *144*, 214108.
101. Ioannidis, E. I.; Gani, T. Z. H.; Kulik, H. J., Molsimplify: A Toolkit for Automating Discovery in Inorganic Chemistry. *J. Comput. Chem.* **2016**, *37*, 2106-2117.
102. Baker, J., An Algorithm for the Location of Transition States. *J. Comput. Chem.* **1986**, *7*, 385-395.
103. Shao, Y.; Gan, Z.; Epifanovsky, E.; Gilbert, A. T.; Wormit, M.; Kussmann, J.; Lange, A. W.; Behn, A.; Deng, J.; Feng, X., Advances in Molecular Quantum Chemistry Contained in the Q-Chem 4 Program Package. *Mol. Phys.* **2015**, *113*, 184-215.
104. Ishida, K.; Morokuma, K.; Komornicki, A., The Intrinsic Reaction Coordinate. An Abinitio Calculation for Hnc->Hcn and H+ Ch4-> Ch4+ H-. *J. Chem. Phys.* **1977**, *66*, 2153-2156.
105. Schmidt, M. W.; Gordon, M. S.; Dupuis, M., The Intrinsic Reaction Coordinate and the Rotational Barrier in Silaethylene. *J. Am. Chem. Soc.* **1985**, *107*, 2585-2589.
106. Fukui, K., Formulation of the Reaction Coordinate. *J. Phys. Chem.* **1970**, *74*, 4161-4163.
107. Fukui, K., The Path of Chemical Reactions-the IRC Approach. *Acc. Chem. Res.* **1981**, *14*, 363-368.

108. Riplinger, C.; Sandhoefer, B.; Hansen, A.; Neese, F., Natural Triple Excitations in Local Coupled Cluster Calculations with Pair Natural Orbitals. *J. Chem. Phys.* **2013**, *139*, 134101.
109. Neese, F., The Orca Program System. *Wiley Interdiscip. Rev.: Comput. Mol. Sci.* **2012**, *2*, 73-78.
110. Stoychev, G. L.; Auer, A. A.; Neese, F., Automatic Generation of Auxiliary Basis Sets. *J. Chem. Theory Comput.* **2017**, *13*, 554-562.
111. Helgaker, T.; Klopper, W.; Koch, H.; Noga, J., Basis-Set Convergence of Correlated Calculations on Water. *J. Chem. Phys.* **1997**, *106*, 9639-9646.
112. Truhlar, D. G., Basis-Set Extrapolation. *Chem. Phys. Lett.* **1998**, *294*, 45-48.
113. Neese, F.; Valeev, E. F., Revisiting the Atomic Natural Orbital Approach for Basis Sets: Robust Systematic Basis Sets for Explicitly Correlated and Conventional Correlated Ab Initio Methods? *J. Chem. Theory Comput.* **2010**, *7*, 33-43.
114. Liakos, D. G.; Neese, F., Interplay of Correlation and Relativistic Effects in Correlated Calculations on Transition-Metal Complexes: The (Cu₂O₂)²⁺ Core Revisited. *J. Chem. Theory Comput.* **2011**, *7*, 1511-1523.
115. Angeli, C.; Cimiraglia, R.; Evangelisti, S.; Leininger, T.; Malrieu, J.-P., Introduction of N-Electron Valence States for Multireference Perturbation Theory. *J. Chem. Phys.* **2001**, *114*, 10252-10264.
116. Weigend, F.; Ahlrichs, R., Balanced Basis Sets of Split Valence, Triple Zeta Valence and Quadruple Zeta Valence Quality for H to Rn: Design and Assessment of Accuracy. *Phys. Chem. Chem. Phys.* **2005**, *7*, 3297-3305.
117. Kupper, C.; Mondal, B.; Serrano-Plana, J.; Klawitter, I.; Neese, F.; Costas, M.; Ye, S.; Meyer, F., Non-Classical Single-State Reactivity of an Oxo-Iron (IV) Complex Confined to Triplet Pathways. *J. Am. Chem. Soc.* **2017**, *139*, 8939-8949.
118. Pierloot, K.; Vancoillie, S., Relative Energy of the High-(T_{2g}⁵) and Low-(A_{1g}¹) Spin States of the Ferrous Complexes [Fe(L)(NHS₄)]: CASPT2 Versus Density Functional Theory. *J. Chem. Phys.* **2008**, *128*, 034104.
119. Mayer, I., Charge, Bond Order and Valence in the Ab Initio Scf Theory. *Chem. Phys. Lett.* **1983**, *97*, 270-274.
120. Mayer, I., Bond Order and Valence: Relations to Mulliken's Population Analysis. *Int. J. Quantum Chem.* **1984**, *26*, 151-154.
121. Lu, T.; Chen, F., Multiwfn: A Multifunctional Wavefunction Analyzer. *J. Comput. Chem.* **2012**, *33*, 580-592.
122. Bridgeman, A. J.; Cavigliasso, G.; Ireland, L. R.; Rothery, J., The Mayer Bond Order as a Tool in Inorganic Chemistry. *J. Chem. Soc., Dalton Trans.* **2001**, 2095-2108.
123. Stevenson, J.; Sorenson, B.; Subramaniam, V. H.; Raiford, J.; Khlyabich, P. P.; Loo, Y.-L.; Clancy, P., Mayer Bond Order as a Metric of Complexation Effectiveness in Lead Halide Perovskite Solutions. *Chem. Mater.* **2016**, *29*, 2435-2444.
124. Reed, A. E.; Weinstock, R. B.; Weinhold, F., Natural Population Analysis. *J. Chem. Phys.* **1985**, *83*, 735-746.
125. Bader, R. F. W., A Quantum Theory of Molecular Structure and Its Applications. *Chem. Rev.* **1991**, *91*, 893-928.
126. NBO6.0., E. D. Glendening, J. K. Badenhoop, A. E. Reed, J. E. Carpenter, J. A. Bohmann, C. M. Morales, C. R. Landis, and F. Weinhold, Theoretical Chemistry Institute, University of Wisconsin, Madison. 2013.
127. Xiao, D. J.; Bloch, E. D.; Mason, J. A.; Queen, W. L.; Hudson, M. R.; Planas, N.; Borycz, J.; Dzubak, A. L.; Verma, P.; Lee, K., Oxidation of Ethane to Ethanol by N₂O in a Metal–Organic Framework with Coordinatively Unsaturated Iron (II) Sites. *Nat. Chem.* **2014**, *6*, 590-595.
128. Sahu, S.; Goldberg, D. P., Activation of Dioxygen by Iron and Manganese Complexes: A Heme and Nonheme Perspective. *J. Am. Chem. Soc.* **2016**, *138*, 11410-11428.
129. Nam, W., Synthetic Mononuclear Nonheme Iron–Oxygen Intermediates. *Acc. Chem. Res.* **2015**, *48*, 2415-2423.

130. Teles, J. H.; Hermans, I.; Franz, G.; Sheldon, R. A., Oxidation. In *Ullmann's Encyclopedia of Industrial Chemistry*, Wiley-VCH Verlag GmbH & Co. KGaA: 2015.
131. Hohenberger, J.; Ray, K.; Meyer, K., The Biology and Chemistry of High-Valent Iron-Oxo and Iron-Nitrido Complexes. *Nat. Commun.* **2012**, *3*, 720.
132. Wang, V. C.-C.; Maji, S.; Chen, P. P.-Y.; Lee, H. K.; Yu, S. S.-F.; Chan, S. I., Alkane Oxidation: Methane Monooxygenases, Related Enzymes, and Their Biomimetics. *Chem. Rev.* **2017**, *117*, 8574-8621.
133. Ye, S.; Geng, C.-Y.; Shaik, S.; Neese, F., Electronic Structure Analysis of Multistate Reactivity in Transition Metal Catalyzed Reactions: The Case of C–H Bond Activation by Non-Heme Iron (IV)–Oxo Cores. *Phys. Chem. Chem. Phys.* **2013**, *15*, 8017-8030.
134. Verma, P.; Vogiatzis, K. D.; Planas, N.; Borycz, J.; Xiao, D. J.; Long, J. R.; Gagliardi, L.; Truhlar, D. G., Mechanism of Oxidation of Ethane to Ethanol at Iron (IV)–Oxo Sites in Magnesium-Diluted Fe₂ (Dobdc). *J. Am. Chem. Soc.* **2015**, *137*, 5770-5781.
135. Schröder, D.; Shaik, S.; Schwarz, H., Two-State Reactivity as a New Concept in Organometallic Chemistry. *Acc. Chem. Res.* **2000**, *33*, 139-145.
136. Hirao, H.; Kumar, D.; Que, L.; Shaik, S., Two-State Reactivity in Alkane Hydroxylation by Non-Heme Iron–Oxo Complexes. *J. Am. Chem. Soc.* **2006**, *128*, 8590-8606.
137. Janardanan, D.; Wang, Y.; Schyman, P.; Que, L.; Shaik, S., The Fundamental Role of Exchange-Enhanced Reactivity in C-H Activation by S=2 Oxo Iron (IV) Complexes. *Angew. Chem. Int. Ed.* **2010**, *49*, 3342-3345.
138. Shaik, S.; Chen, H.; Janardanan, D., Exchange-Enhanced Reactivity in Bond Activation by Metal-Oxo Enzymes and Synthetic Reagents. *Nat. Chem.* **2011**, *3*, 19-27.
139. Janardanan, D.; Usharani, D.; Chen, H.; Shaik, S., Modeling C–H Abstraction Reactivity of Nonheme Fe (IV) O Oxidants with Alkanes: What Role Do Counter Ions Play? *J. Phys. Chem. Lett.* **2011**, *2*, 2610-2617.
140. Lundberg, M.; Siegbahn, P. E. M., Quantifying the Effects of the Self-Interaction Error in DFT: When Do the Delocalized States Appear? *J. Chem. Phys.* **2005**, *122*, 224103.
141. Kozuch, S.; Shaik, S., How to Conceptualize Catalytic Cycles? The Energetic Span Model. *Acc. Chem. Res.* **2010**, *44*, 101-110.
142. Hirao, H.; Ng, W. K. H.; Moeljadi, A. M. P.; Bureekaew, S., Multiscale Model for a Metal–Organic Framework: High-Spin Rebound Mechanism in the Reaction of the Oxoiron (IV) Species of Fe-Mof-74. *ACS Catal.* **2015**, *5*, 3287-3291.
143. Adamo, C.; Barone, V., Toward Reliable Density Functional Methods without Adjustable Parameters: The PBE0 Model. *J. Chem. Phys.* **1999**, *110*, 6158-6170.
144. Blomberg, M. R. A.; Siegbahn, P. E. M., Quantum Chemistry Applied to the Mechanisms of Transition Metal Containing Enzymes—Cytochrome C Oxidase, a Particularly Challenging Case. *J. Comput. Chem.* **2006**, *27*, 1373-1384.
145. Karen, P.; McArdle, P.; Takats, J., Toward a Comprehensive Definition of Oxidation State (Iupac Technical Report). *Pure Appl. Chem.* **2014**, *86*, 1017-1081.
146. Merrick, J. P.; Moran, D.; Radom, L., An Evaluation of Harmonic Vibrational Frequency Scale Factors. *J. Phys. Chem. A* **2007**, *111*, 11683-11700.
147. Tripp, B. C.; Smith, K.; Ferry, J. G., Carbonic Anhydrase: New Insights for an Ancient Enzyme. *J. Biol. Chem.* **2001**, *276*, 48615-48618.
148. Schröder, D.; Schwarz, H.; Schenk, S.; Anders, E., A Gas-Phase Reaction as a Functional Model for the Activation of Carbon Dioxide by Carbonic Anhydrase. *Angew. Chem. Int. Ed.* **2003**, *42*, 5087-5090.
149. Kulik, H. J.; Wong, S. E.; Baker, S. E.; Valdez, C. A.; Satcher, J. H.; Aines, R. D.; Lightstone, F. C., Developing an Approach for First-Principles Catalyst Design: Application to Carbon-Capture Catalysis. *Acta Crystallogr., Sect. C: Struct. Chem.* **2014**, *70*, 123-131.
150. Fernández, I.; Bickelhaupt, F. M., The Activation Strain Model and Molecular Orbital Theory: Understanding and Designing Chemical Reactions. *Chem. Soc. Rev.* **2014**, *43*, 4953-4967.

151. van Zeist, W.-J.; Bickelhaupt, F. M., The Activation Strain Model of Chemical Reactivity. *Org. Biomol. Chem.* **2010**, *8*, 3118-3127.
152. de Jong, G. T.; Bickelhaupt, F. M., Transition-State Energy and Position Along the Reaction Coordinate in an Extended Activation Strain Model. *ChemPhysChem* **2007**, *8*, 1170-1181.
153. Diefenbach, A.; Bickelhaupt, F. M., Activation of H–H, C–H, C–C, and C–Cl Bonds by Pd(0). Insight from the Activation Strain Model. *J. Phys. Chem. A* **2004**, *108*, 8460-8466.
154. Liu, F.; Paton, R. S.; Kim, S.; Liang, Y.; Houk, K., Diels–Alder Reactivities of Strained and Unstrained Cycloalkenes with Normal and Inverse-Electron-Demand Dienes: Activation Barriers and Distortion/Interaction Analysis. *J. Am. Chem. Soc.* **2013**, *135*, 15642-15649.
155. Green, A. G.; Liu, P.; Merlic, C. A.; Houk, K., Distortion/Interaction Analysis Reveals the Origins of Selectivities in Iridium-Catalyzed C–H Borylation of Substituted Arenes and 5-Membered Heterocycles. *J. Am. Chem. Soc.* **2014**, *136*, 4575-4583.
156. Yu, P.; Yang, Z.; Liang, Y.; Hong, X.; Li, Y.; Houk, K., Distortion-Controlled Reactivity and Molecular Dynamics of Dehydro-Diels–Alder Reactions. *J. Am. Chem. Soc.* **2016**, *138*, 8247-8252.
157. Kim, J. Y.; Steeves, A. H.; Kulik, H. J., Harnessing Organic Ligand Libraries for First-Principles Inorganic Discovery: Indium Phosphide Quantum Dot Precursor Design Strategies. *Chem. Mater.* **2017**, *29*, 3632-3643.
158. Neese, F.; Liakos, D. G.; Ye, S., Correlated Wavefunction Methods in Bioinorganic Chemistry. *J. Biol. Inorg. Chem.* **2011**, *16*, 821-829.
159. Ye, S.; Riplinger, C.; Hansen, A.; Krebs, C.; Bollinger, J. M.; Neese, F., Electronic Structure Analysis of the Oxygen-Activation Mechanism by FeII- and α -Ketoglutarate (Akg)-Dependent Dioxygenases. *Chem. Eur. J.* **2012**, *18*, 6555-6567.
160. Chen, H.; Lai, W.; Shaik, S., Exchange-Enhanced H-Abstraction Reactivity of High-Valent Nonheme Iron(IV)-Oxo from Coupled Cluster and Density Functional Theories. *J. Phys. Chem. Lett.* **2010**, *1*, 1533-1540.
161. Carter, E. A.; Goddard III, W. A., Relationships between Bond Energies in Coordinatively Unsaturated and Coordinatively Saturated Transition-Metal Complexes: A Quantitative Guide for Single, Double, and Triple Bonds. *J. Phys. Chem.* **1988**, *92*, 5679-5683.
162. Cotton, F. A.; Wilkinson, G., *Advanced Inorganic Chemistry, 5th Edition*. Wiley: New York, 1988.
163. Raebiger, H.; Lany, S.; Zunger, A., Charge Self-Regulation Upon Changing the Oxidation State of Transition Metals in Insulators. *Nature* **2008**, *453*, 763.
164. Aullón, G.; Alvarez, S., Oxidation States, Atomic Charges and Orbital Populations in Transition Metal Complexes. *Theor. Chem. Acc.* **2009**, *123*, 67-73.
165. Takahashi, A.; Yamaki, D.; Ikemura, K.; Kurahashi, T.; Ogura, T.; Hada, M.; Fujii, H., Effect of the Axial Ligand on the Reactivity of the Oxoiron(IV) Porphyrin π -Cation Radical Complex: Higher Stabilization of the Product State Relative to the Reactant State. *Inorg. Chem.* **2012**, *51*, 7296-7305.
166. Peterson, A. A.; Nørskov, J. K., Activity Descriptors for CO₂ Electroreduction to Methane on Transition-Metal Catalysts. *J. Phys. Chem. Lett.* **2012**, *3*, 251-258.
167. Mavros, M. G.; Tsuchimochi, T.; Kowalczyk, T.; McIsaac, A.; Wang, L.-P.; Van Voorhis, T., What Can Density Functional Theory Tell Us About Artificial Catalytic Water Splitting? *Inorg. Chem.* **2014**, *53*, 6386-6397.
168. Zagal, J. H.; Koper, M., Reactivity Descriptors for the Activity of Molecular Mn⁴ Catalysts for the Oxygen Reduction Reaction. *Angew. Chem. Int. Ed.* **2016**, *55*, 14510-14521.
169. Fukui, K., Role of Frontier Orbitals in Chemical Reactions. *Science* **1982**, *218*, 747-754.
170. Janak, J. F., Proof That $dE/dn_i = \epsilon_i$ in Density-Functional Theory. *Phys. Rev. B* **1978**, *18*, 7165-7168.
171. Schröder, D.; Schwarz, H., FeO⁺ Activates Methane. *Angew. Chem. Int. Ed.* **1990**, *29*, 1433-1434.

172. Schroeder, D.; Fiedler, A.; Hrusak, J.; Schwarz, H., Experimental and Theoretical Studies toward a Characterization of Conceivable Intermediates Involved in the Gas-Phase Oxidation of Methane by Bare FeO⁺. Generation of Four Distinguishable [Fe, C, H₄, O]⁺ Isomers. *J. Am. Chem. Soc.* **1992**, *114*, 1215-1222.
173. Schröder, D.; Schwarz, H.; Clemmer, D. E.; Chen, Y.; Armentrout, P. B.; Baranov, V. I.; Böhme, D. K., Activation of Hydrogen and Methane by Thermalized FeO⁺ in the Gas Phase as Studied by Multiple Mass Spectrometric Techniques. *Int. J. Mass Spectrom. Ion Processes* **1997**, *161*, 175-191.
174. Aguirre, F.; Husband, J.; Thompson, C. J.; Stringer, K. L.; Metz, R. B., Electronic Spectroscopy of Intermediates Involved in the Conversion of Methane to Methanol by FeO⁺. *J. Chem. Phys.* **2002**, *116*, 4071-4078.
175. Altinay, G.; Citir, M.; Metz, R. B., Vibrational Spectroscopy of Intermediates in Methane-to-Methanol Conversion by FeO⁺. *J. Phys. Chem. A* **2010**, *114*, 5104-5112.
176. Ard, S. G.; Melko, J. J.; Ushakov, V. G.; Johnson, R.; Fournier, J. A.; Shuman, N. S.; Guo, H.; Troe, J.; Viggiano, A. A., Activation of Methane by FeO⁺: Determining Reaction Pathways through Temperature-Dependent Kinetics and Statistical Modeling. *J. Phys. Chem. A* **2014**, *118*, 2029-2039.
177. Yoshizawa, K.; Shiota, Y.; Yamabe, T., Abstraction of the Hydrogen Atom of Methane by Iron–Oxo Species: The Concerted Reaction Path Is Energetically More Favorable. *Organometallics* **1998**, *17*, 2825-2831.
178. Brönstrup, M.; Schröder, D.; Schwarz, H., Reactions of Bare FeO⁺ with Element Hydrides Ehn (E= C, N, O, F, Si, P, S, Cl). *Chem. Eur. J.* **1999**, *5*, 1176-1185.
179. Yoshizawa, K.; Shiota, Y.; Yamabe, T., Intrinsic Reaction Coordinate Analysis of the Conversion of Methane to Methanol by an Iron–Oxo Species: A Study of Crossing Seams of Potential Energy Surfaces. *J. Chem. Phys.* **1999**, *111*, 538-545.
180. Shiota, Y.; Yoshizawa, K., Methane-to-Methanol Conversion by First-Row Transition-Metal Oxide Ions: Sco⁺, Tio⁺, Vo⁺, Cro⁺, Mno⁺, FeO⁺, CoO⁺, Nio⁺, and CuO⁺. *J. Am. Chem. Soc.* **2000**, *122*, 12317-12326.
181. Wang, Y.; Sun, X.; Zhang, J.; Li, J., A Theoretical Study on Methane C-H Bond Activation by Bare [FeO]^{+0/-}. *J. Phys. Chem. A* **2017**, *121*, 3501-3514.
182. Kramida, A., Ralchenko, Yu., Reader, J. and NIST ASD Team NIST Atomic Spectra Database (Version 5.3), [Online]. <http://physics.nist.gov/asd> (accessed June 08, 2017).

